Electronic Supplementary Material (ESI) for Sustainable Energy & Fuels.


**Supporting information**

# Effect of yttrium, ytterbium with tungsten co-doping on light absorption and charge transport properties of bismuth vanadate photoanodes to achieve superior photoelectrochemical water splitting

Umesh Prasad[1]*, Jyoti Prakash[1] and Arunachala M. Kannan[1]*
[1] The Polytechnic School, Ira A. Fulton Schools of Engineering, Arizona State University, Mesa, AZ 85212, USA

*Corresponding Author: amk@asu.edu (AM Kannan)/ uprasad1@asu.edu (Umesh Prasad)

**PEC measurement, potential conversion, Impedance measurement, electrochemical surface area and Space width charge region calculation**

The exposed backside area of photoanode for light illumination was 1 $cm^2$. For 1 sun illumination, a solar simulator (Newport 67005) equipped with an AM 1.5G filter used as a light source which is integrated with potentiostat/galvanostatic (PARSTAT-2273). The photoanodes were mounted perpendicular to the light source to maintain measurement accuracy. 1 sun illimitation intensity was assured in Figure S1a which shows solar light intensity calibration with the X-Y direction at 7 cm from the light source.

The light intensity distribution for the solar simulator (Newport Model # 67005) was determined using a lux meter (Silicon photo-detector; Extech Model # SDL400) using insulating tape as a black mask with hole of 1 cm x 0.8 cm (size of exposed thin film) and calibrated with the X-Y direction at 7 cm from the light source. It was validated from the Figure S1a that the light illumination is 100 $mW.cm^{-2}$ irradiating on the photoanode surface (geometrical area = 1 $cm^2$) after placing the sample at the center. Slight error in sample placement will affect (reduce) the light illumination intensity on the photoanode surface. An assumed experimental error in the placement of photoanodes are in the order of 0.25 cm which provides a representative value to the alignment of the photoanode with the naked eye. This led to the light illumination intensity variation in the range of 95-100 $mW.cm^{-2}$ which is small enough to avoid. The PEC measurement was conducted in the open environment inside the lab. The other errors such as reflection from glass-air media, glass-water interfaces and the electrolyte solution media during measurements would cause further decrease in the actual light illumination intensity below 1 sun. For clarity, we have placed the sample approximately 2 cm from the edge of the glass. It is worth noting that we followed the protocol in the literature[1].

The potential was converted to reverse hydrogen electrode (RHE) as given relationship (eq 1).

$$E_{RHE} = {E_{SCE}}^{0} + E_{SCE} + 0.059\, pH \quad (1)$$

$$Where\ \ {E_{SCE}}^{0} = 0.2415\ V\ vs.\ RHE, at\ 298\ K$$

Electrochemical Impedance measurement was carried out in frequency range 100 mHz to 100 kHz with AC amplitude of 20 mV at 1.23 V vs RHE under 1 sun illumination and using 0.1 M $K_2HPO_4$ electrolyte (pH 8.0). Resistance and capacitance values were estimated by curve fitting using Randles circuits in software EC-Lab v11.20 . Electrochemical surface area (ECSA) was estimated by analyzing current voltammetry (CV) in the dark (non-faradaic zone) at various scan rate as given in litrature[2]. Flat band (onset) potential was measured by Mott–Schottky at 1 kHz in dark with AC amplitude of 20 mV at 1.23 V vs RHE in 0.1 M $K_2HPO_4$ electrolyte (pH 8.0) by relationship given in eq (2)[3].

$$\frac{1}{C^2} = \frac{2}{(\varepsilon\varepsilon_0 A^2 e N_D)}\left(V_{app} - V_{FB} - \frac{K_B T}{e}\right) \quad (2)$$

Where, C is capacitance in space charge region; ε is relative permeability which is taken 68 for the calculation; $\varepsilon_0$ is vacuum permeability ($8.8 \times 10^{-12}$ F $m^{-1}$); A ($cm^2$) is area of photoanode thin film; e is charge of electron ($1.602 \times 10^{-19}$ C); $N_D$ is number of charge carrier per $cm^{-3}$ and estimated from Mott-Schottky measurement plot (Table S3); $V_{app}$ ( vs RHE) applied potential; $V_{FB}$ flat band potential estimated from Mott-Schottky plot; $K_B$ Boltzmann constant (1.38 × 10-23 $JK^{-1}$); T (K) is the temperature at which measurement performed (298K). Width space charge region ($W_{SCL}$) or depletion layer was estimated from eq (3)[3].

$$W_{SCL} = \sqrt{\frac{2\varepsilon\varepsilon_0}{(A^2 e N_D)}(V_{app} - V_{FB} - \frac{K_B T}{e})} \quad (3)$$

**Theoretical photocurrent calculation:**

Calculate light harvesting efficiency (LHE) which is also known as absorption efficiency $\phi_{abs}$ from the absorption by given relationship (eq 4)

$$LHE = 1 - 10^{-A(\lambda)} = \phi_{abs} \quad (4)$$

A: absorbance with wavelength ($\lambda$)

In the next step photon energy and photon flux calculated from AM1.5G solar irradiance with wavelength by following relation (eq 3-5).

$$E(\lambda) = h \times C/\lambda \quad (5)$$

$E(\lambda)$:$photon\ energy$ $h$:$Plank\ constant$ $C$:$speed\ of\ the\ light$

$$Number\ of\ photons = h \times C/\lambda \quad (6)$$

$$Photons\ flux\ (\phi(\lambda)) = P(\lambda)/E(\lambda) \quad (7)$$

Finally, theoretical photocurrent calculated assuming 100% incident to photon conversion efficiency (IPCE) and by following relationship[4,5].

$$J_{theoretical} = \int_{\lambda_1}^{\lambda_2} e \times \phi(\lambda) \times LHE \times d\lambda \quad (8)$$

**Charge separation and charge transfer efficiency calculation:**

Theoretical photocurrent undergoes two major losses bulk and surface recombination which are known as charge separation ($\phi_{sep}$) and charge transfer or charge injection efficiency ($\phi_{trans}$), given relationship eq (9).

$$J_{H_2O} = J_{theoretical} \times \phi_{sep} \times \phi_{trans} \quad (9)$$

The transfer efficiency is almost 100% in the presence of hole scavengers, which is given by relationship eq (10)[5].

$$J_{Na_2SO_3} = J_{theoretical} \times \phi_{trans} \quad (10)$$

Now, $\phi_{sep}$ and $\phi_{trans}$ can be calculated using eq (8-10)

**Charge IPCE and APCE calculation:**

PCD ($J_{mono}$) was measured at different wavelength using light monochromator (Newport CS-130) and PARSTAT-2273 galvanostat/potentiostat in 0.1 M $K_2HPO_4$ electrolyte (pH 8.0). Light intensity ($P_{mono}$)coming out of monochromator was measure using power meter (Newport PMKIT-05-01). IPEC was measured by relationship given in eq (11).

$$IPCE = \frac{Number\ of\ electrons}{Number\ of\ photons} = \frac{J_{mono} \times h \times C}{P_{mono} \times \lambda} \quad (11)$$

APCE (absorbed photon-to-current conversion efficiency) is calculated as given relationship in eq (12)

$$APCE = \frac{IPCE}{LHE} \quad (12)$$

**Integrated current calculation:**

Integrated current ($J_{integrated}$) calculated using eq (4-7) and relationship given in eq (13)

$$J_{Integrated} = \int_{\lambda_1}^{\lambda_2} e \times \phi(\lambda) \times IPCE \times LHE \times d\lambda \quad (13)$$

**Band bending calculation:**

Total amount of band bending at WO3 and BiVO4 interface is calculated based on the eq (14)[6].

$$\Delta E = E_{F,WO_3} - E_{F,(Y,W):BiVO_4} = k_B T ln\left(\frac{N_{D,(Y,W):BiVO_4}}{N_{D,WO_3}}\right)$$

Where, $E_{F,WO_3}$ and $E_{F,(Y,W):BiVO_4}$ are the Fermi energy leves of $WO_3$ and $(Y,W):BiVO_4$ film respectively.

$k_B$ is Boltsmann constant, $T$ is the temperature and $N_{D,WO_3}$ & $N_{D,(Y,W):BiVO_4}$ are the charge carrier densities for $WO_3$ and $(Y,W):BiVO_4$ film respectively.

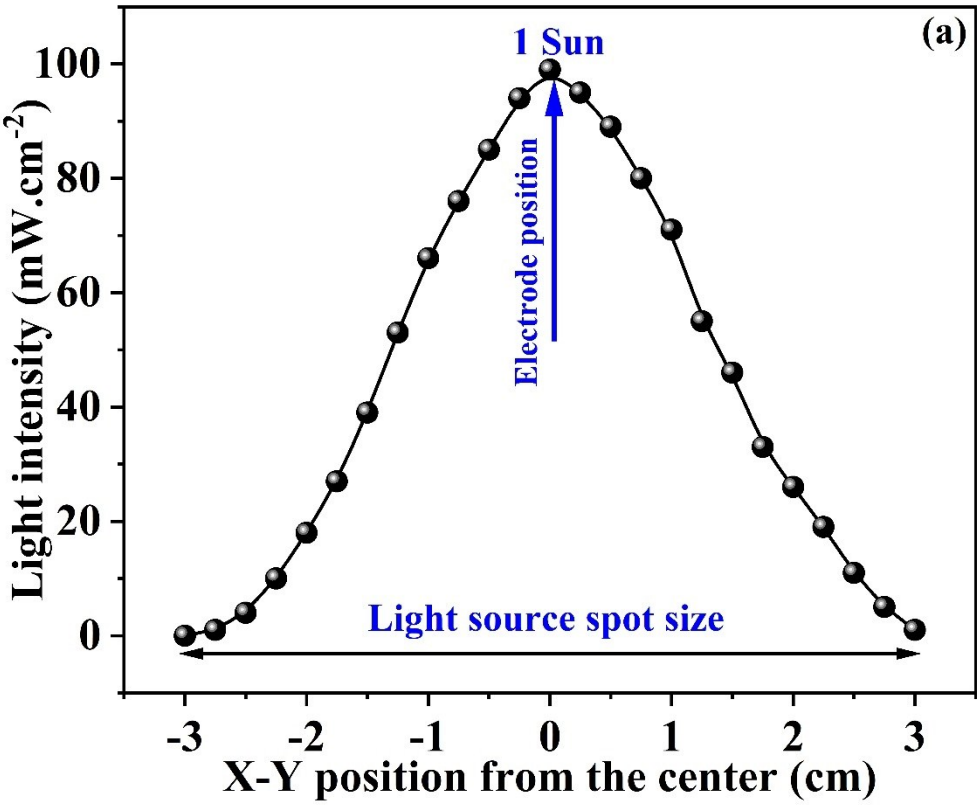
(a)
1 Sun
Electrode position
Light source spot size
Light intensity (mW.cm-2)
X-Y position from the center (cm)
100
80
60
40
20
0
-3
-2
-1
0
1
2
3

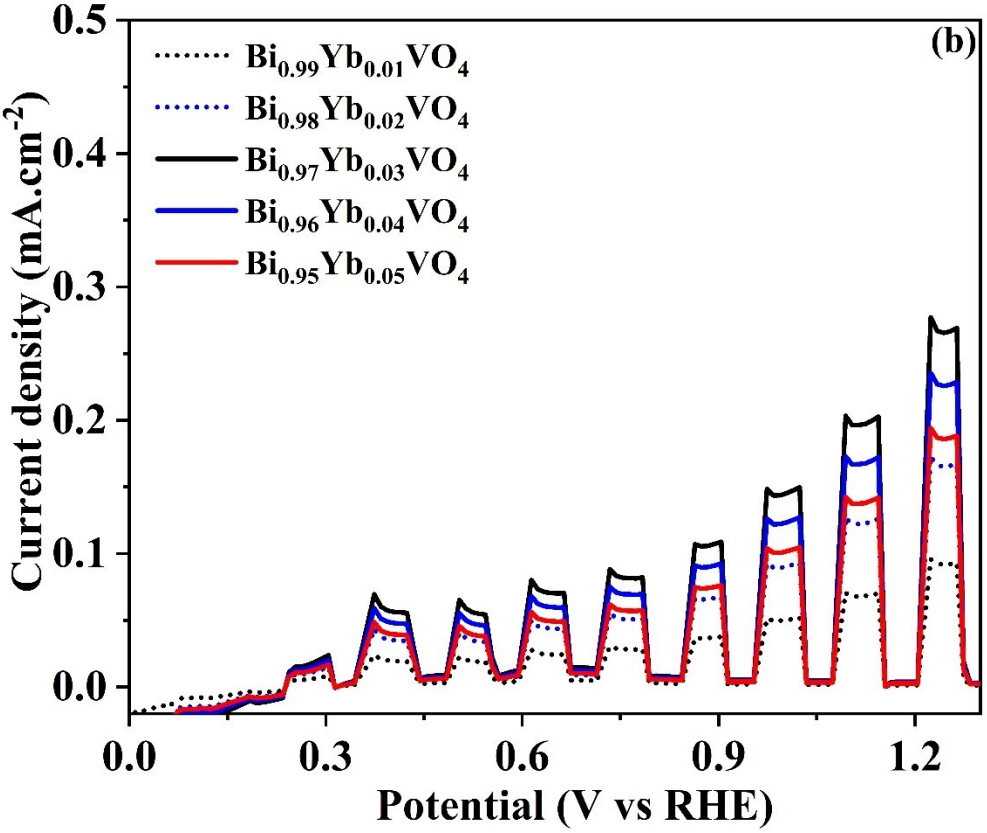
(b)
Bi0.99Yb0.01VO4
Bi0.98Yb0.02VO4
Bi0.97Yb0.03VO4
Bi0.96Yb0.04VO4
Bi0.95Yb0.05VO4
Current density (mA.cm-2)
Potential (V vs RHE)
0.0
0.1
0.2
0.3
0.4
0.5
0.0
0.3
0.6
0.9
1.2

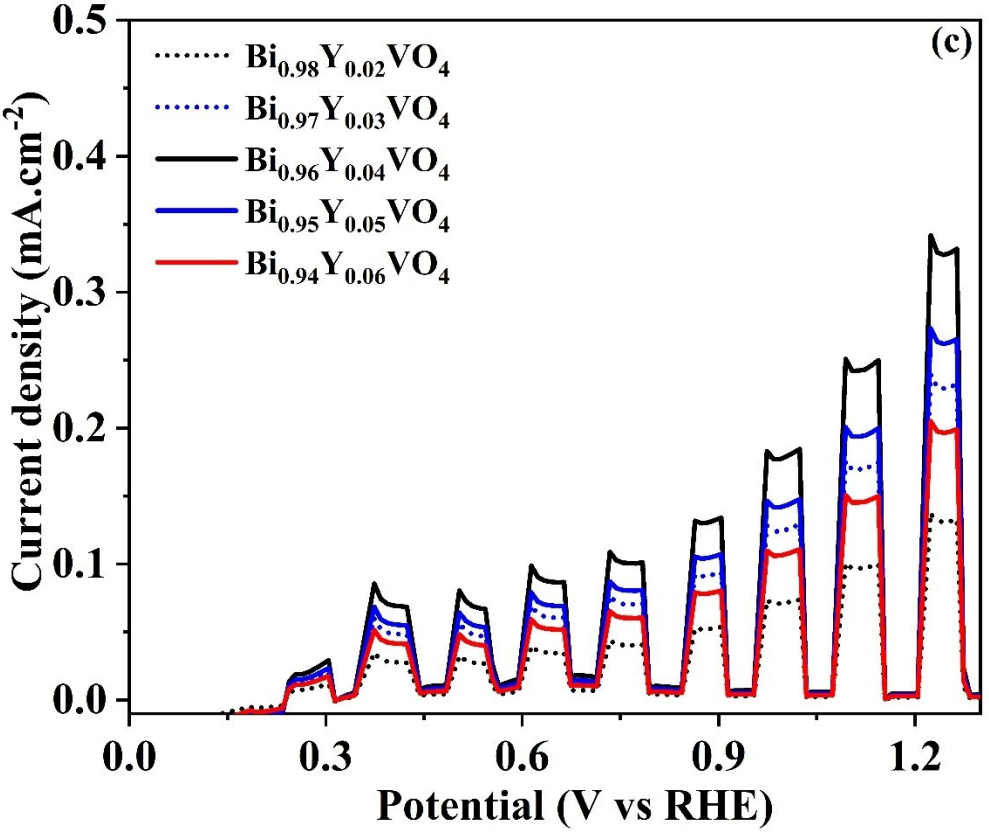


*Figure S1 (a) Solar light intensity calibration chart with the X-Y direction at 7 cm from the light source. Linear sweep voltammetry (LSV) curves for (b) Yb (1 – 5%), (c) Y (2 – 6%) doped $BiVO_4$.*

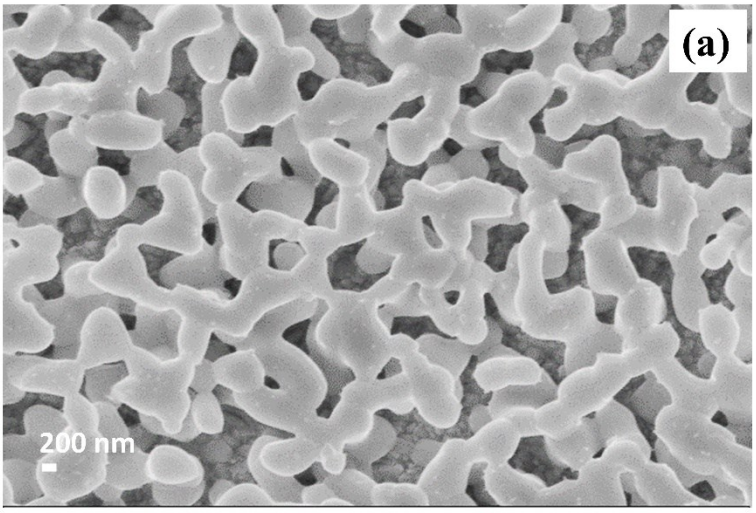
(a)
200 nm

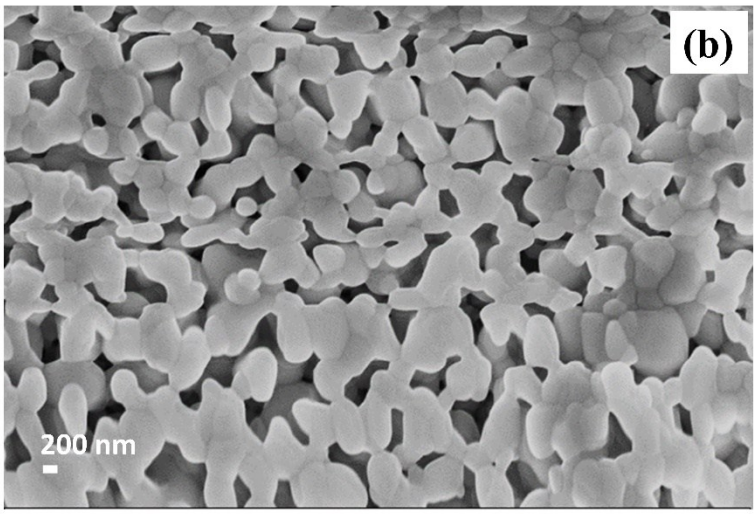
(b)
200 nm

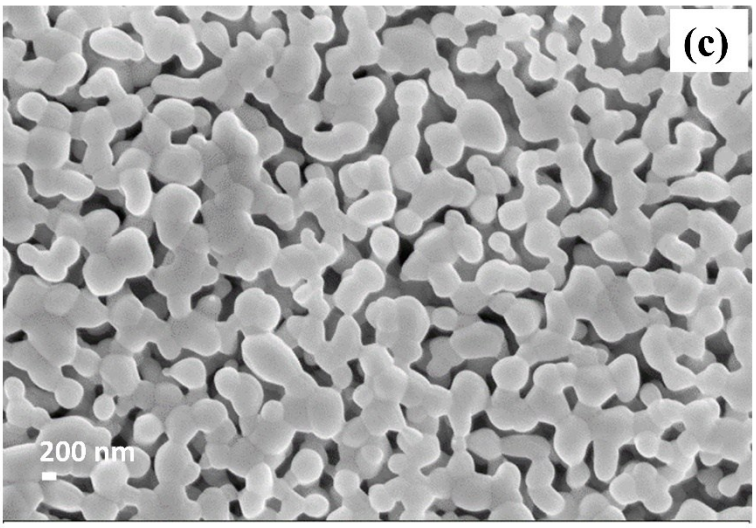
(c)
200 nm

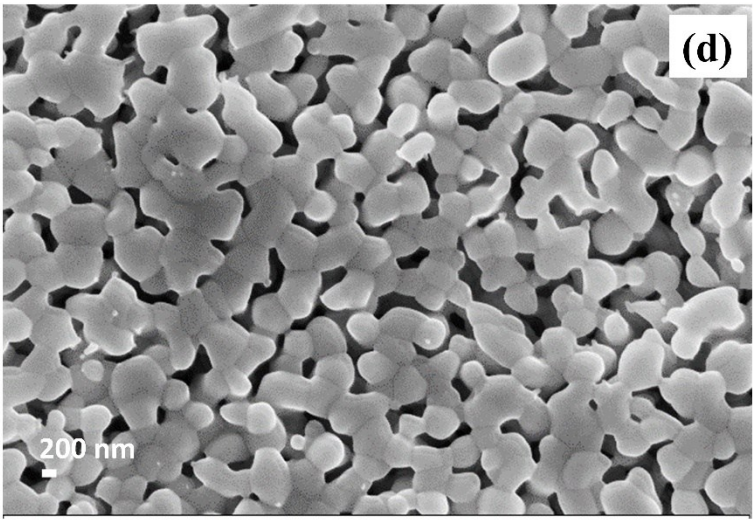
(d)
200 nm

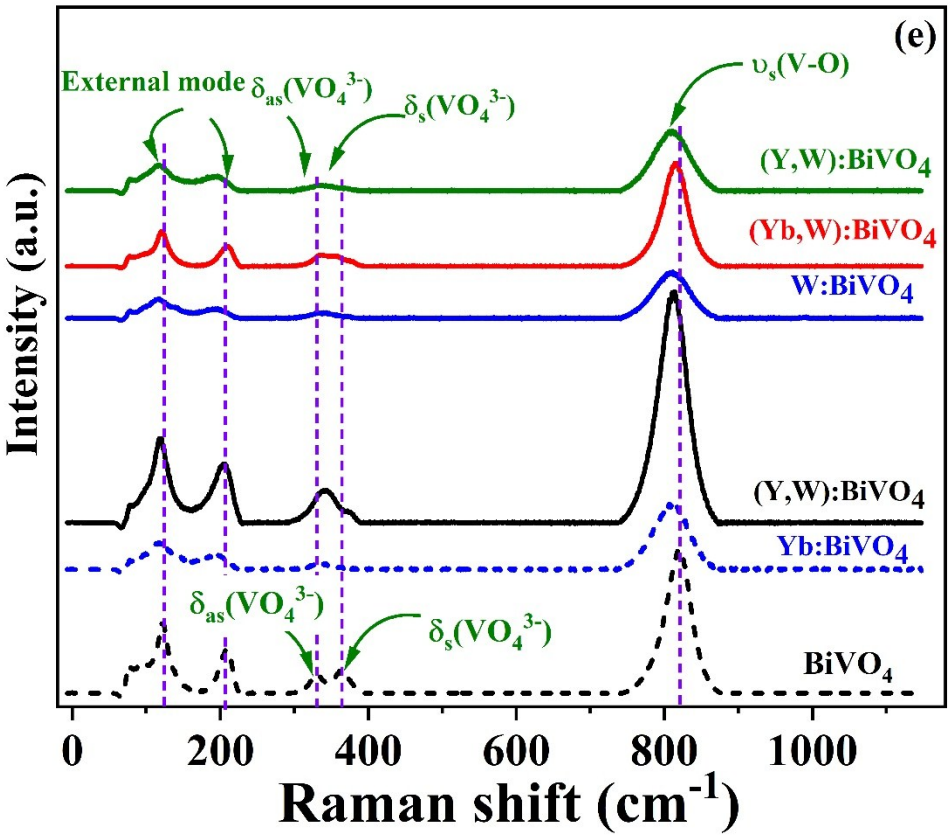
(e)
External mode
$\delta_{as}(VO_4^{3-})$
$\delta_s(VO_4^{3-})$
$\upsilon_s$(V-O)
(Y,W):BiVO$_4$
(Yb,W):BiVO$_4$
W:BiVO$_4$
(Y,W):BiVO$_4$
Yb:BiVO$_4$
$\delta_{as}(VO_4^{3-})$
$\delta_s(VO_4^{3-})$
BiVO$_4$
Intensity (a.u.)
0
200
400
600
800
1000
Raman shift (cm$^{-1}$)

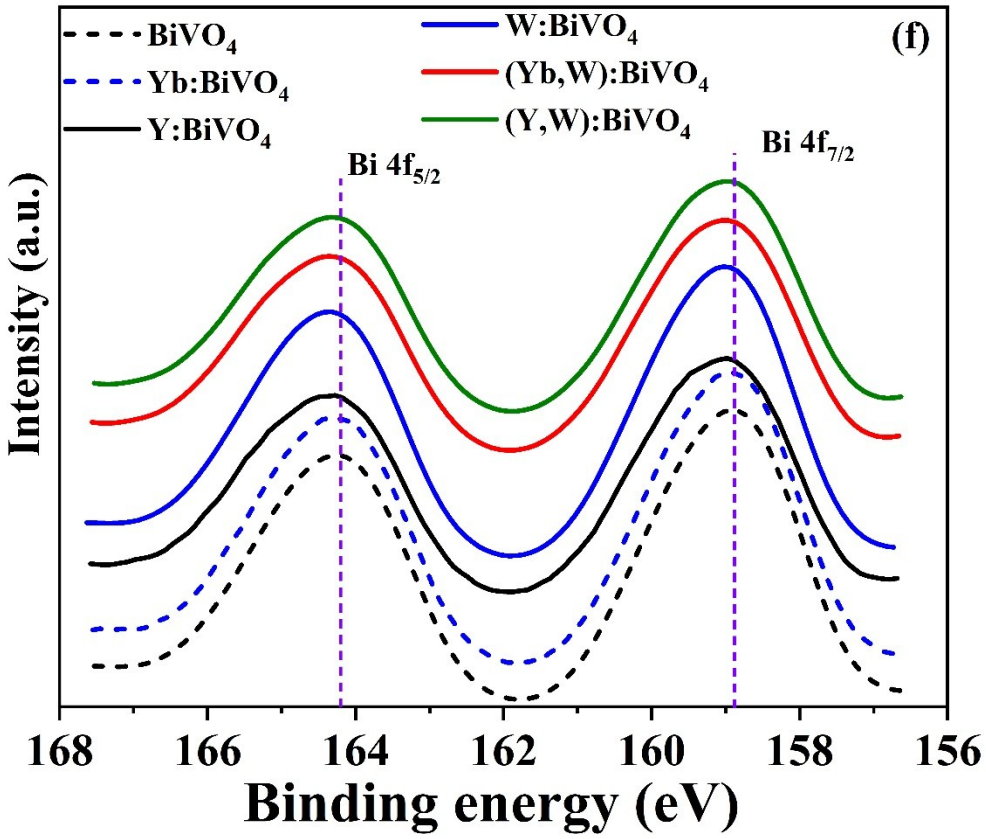
BiVO4
Yb:BiVO4
Y:BiVO4
W:BiVO4
(Yb,W):BiVO4
(Y,W):BiVO4
(f)
Bi 4f5/2
Bi 4f7/2
Intensity (a.u.)
168
166
164
162
160
158
156
Binding energy (eV)

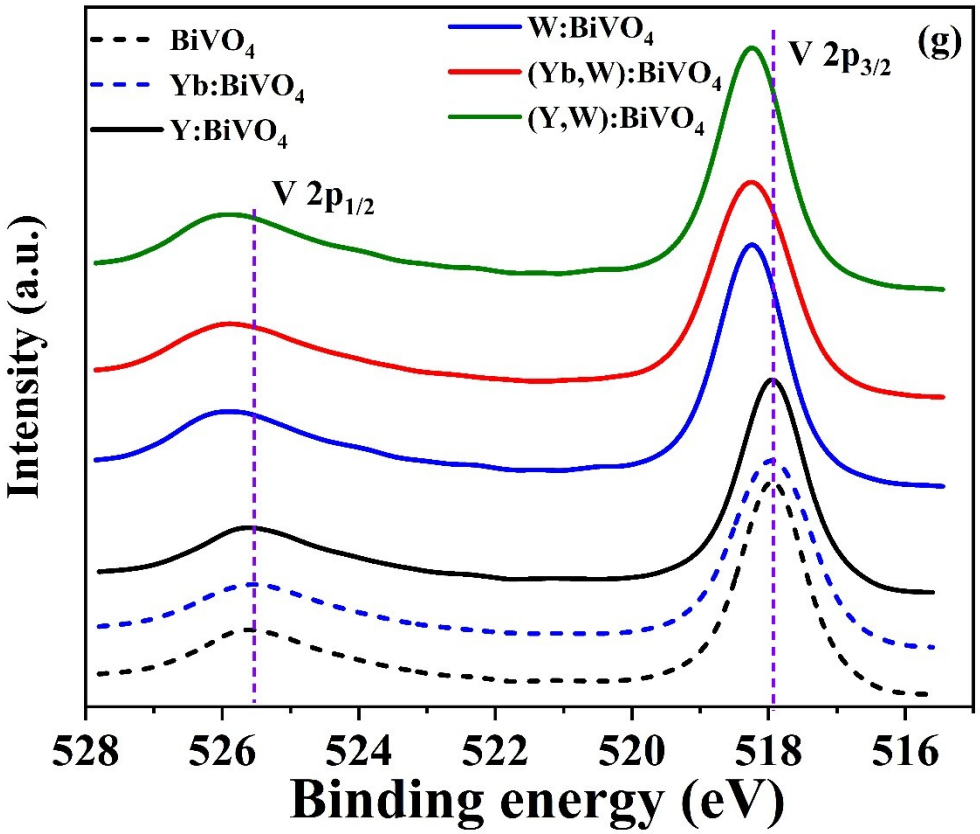
BiVO4
Yb:BiVO4
Y:BiVO4
W:BiVO4
(Yb,W):BiVO4
(Y,W):BiVO4
(g)
V 2p3/2
V 2p1/2
Intensity (a.u.)
528
526
524
522
520
518
516
Binding energy (eV)

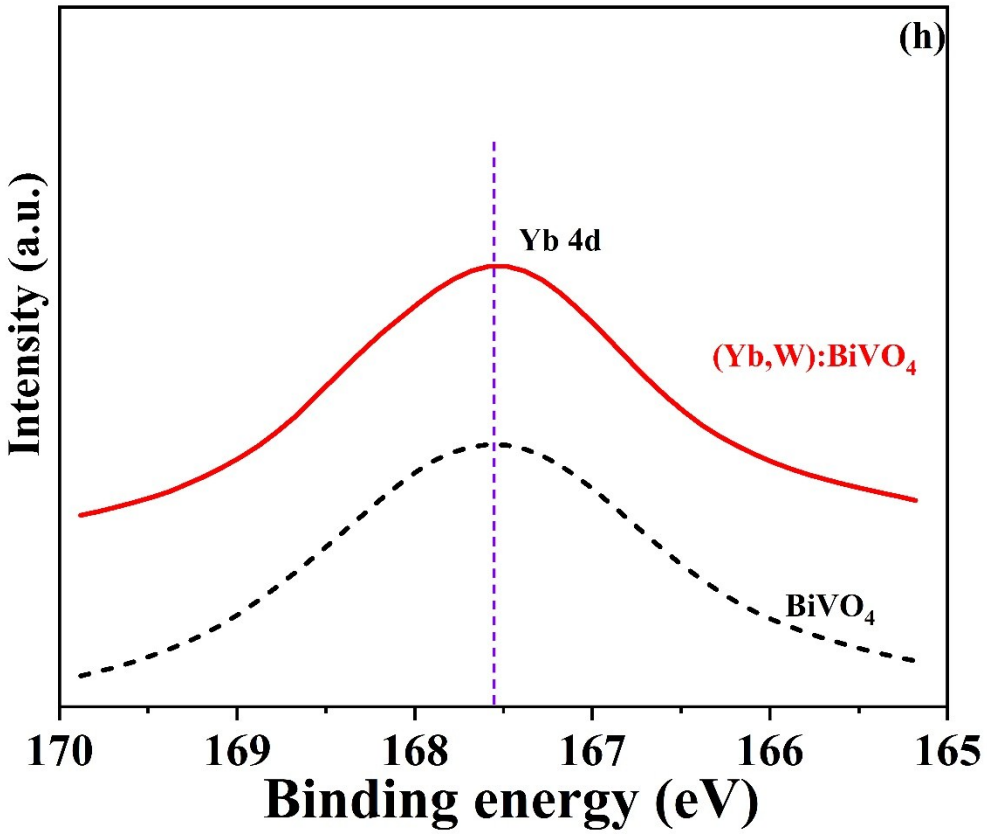
(h)
Intensity (a.u.)
Yb 4d
(Yb,W):BiVO4
BiVO4
170
169
168
167
166
165
Binding energy (eV)

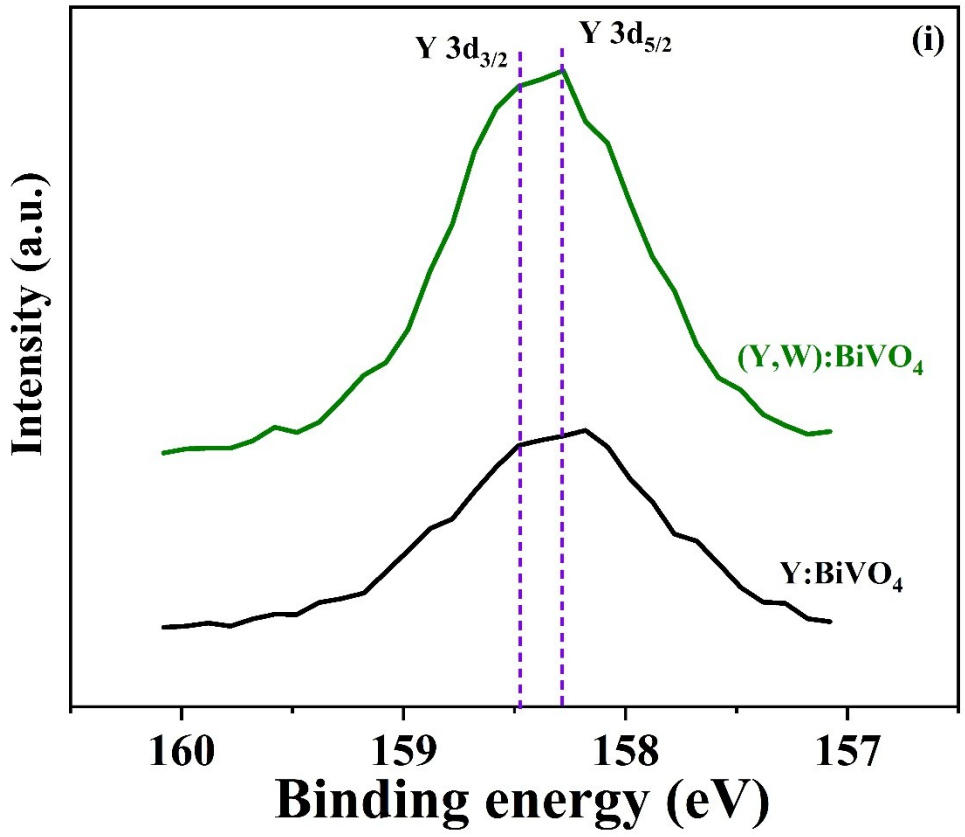
Y 3d3/2
Y 3d5/2
(i)
(Y,W):BiVO4
Y:BiVO4
Intensity (a.u.)
160
159
158
157
Binding energy (eV)

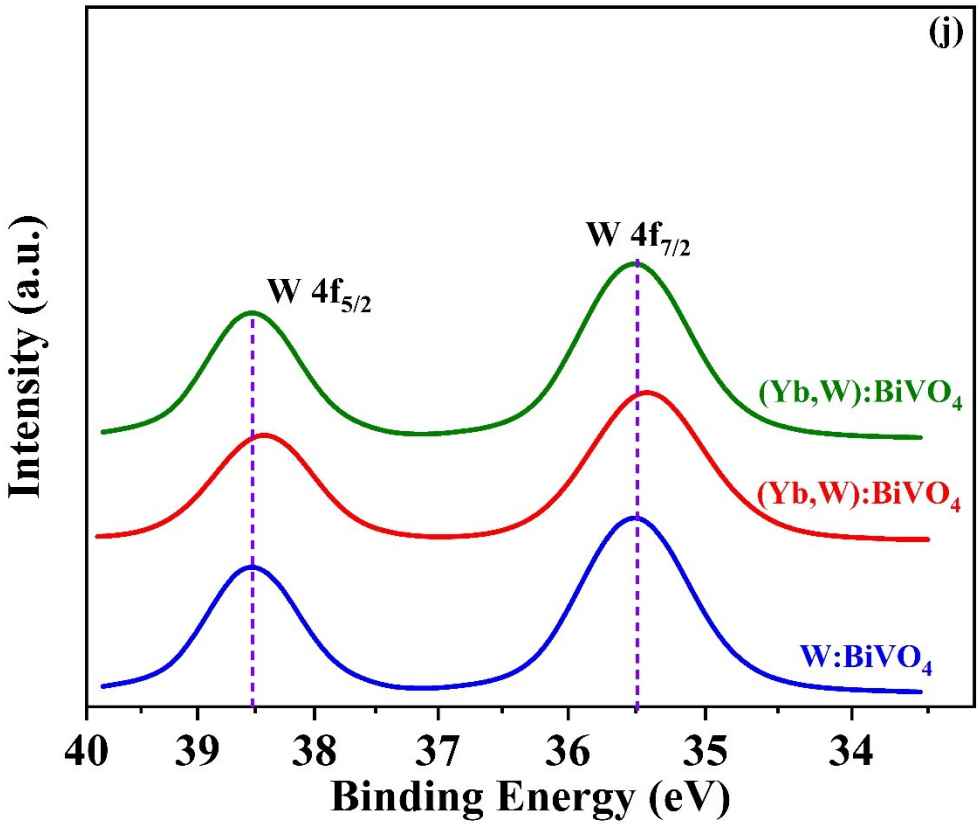


*Figure S2 SEM images of (a) $BiVO_4$ (b) $Yb:BiVO_4$ (c) $Y:BiVO_4$ (d) $W:BiVO_4$. (e) Raman spectra of pristine $BiVO_4$, $Yb:BiVO_4$, $Y:BiVO_4$, $W:BiVO_4$, (Yb,W): $BiVO_4$ and (Y,W):$BiVO_4$ photoanodes. XPS spectra of (f) Bi 4f, (g) V 2p, (h) Yb 4d, (i) Y 3d and (j) W 4f.*

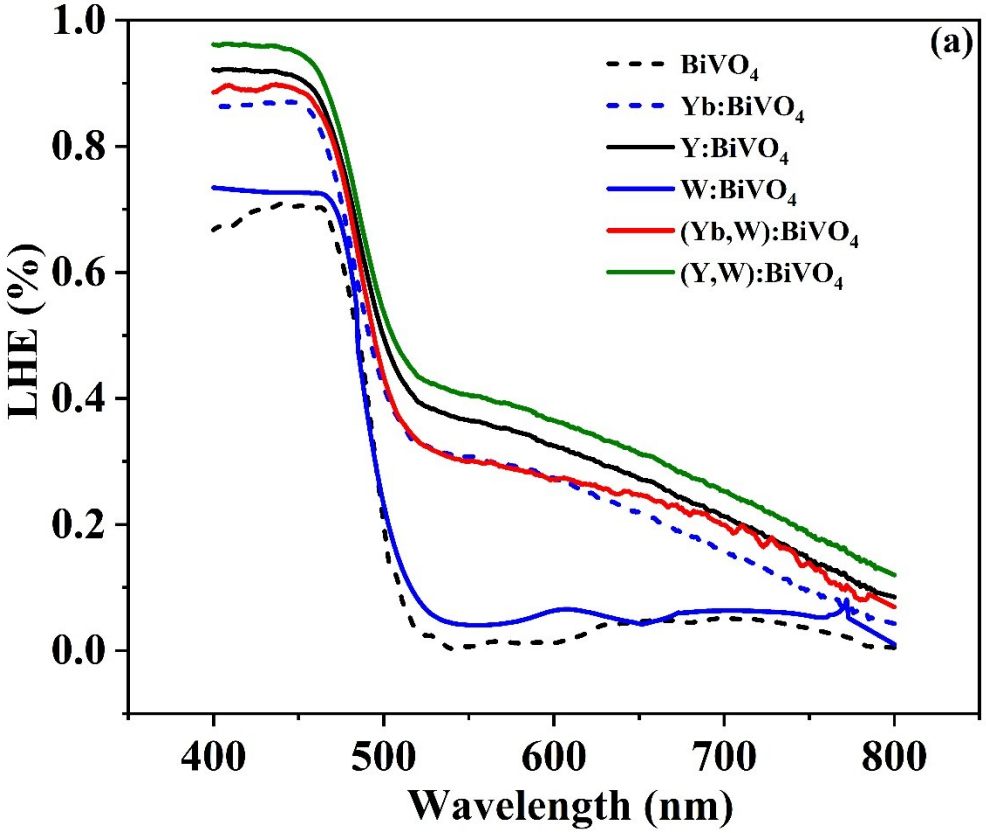
(a)
BiVO4
Yb:BiVO4
Y:BiVO4
W:BiVO4
(Yb,W):BiVO4
(Y,W):BiVO4
LHE (%)
1.0
0.8
0.6
0.4
0.2
0.0
400
500
600
700
800
Wavelength (nm)

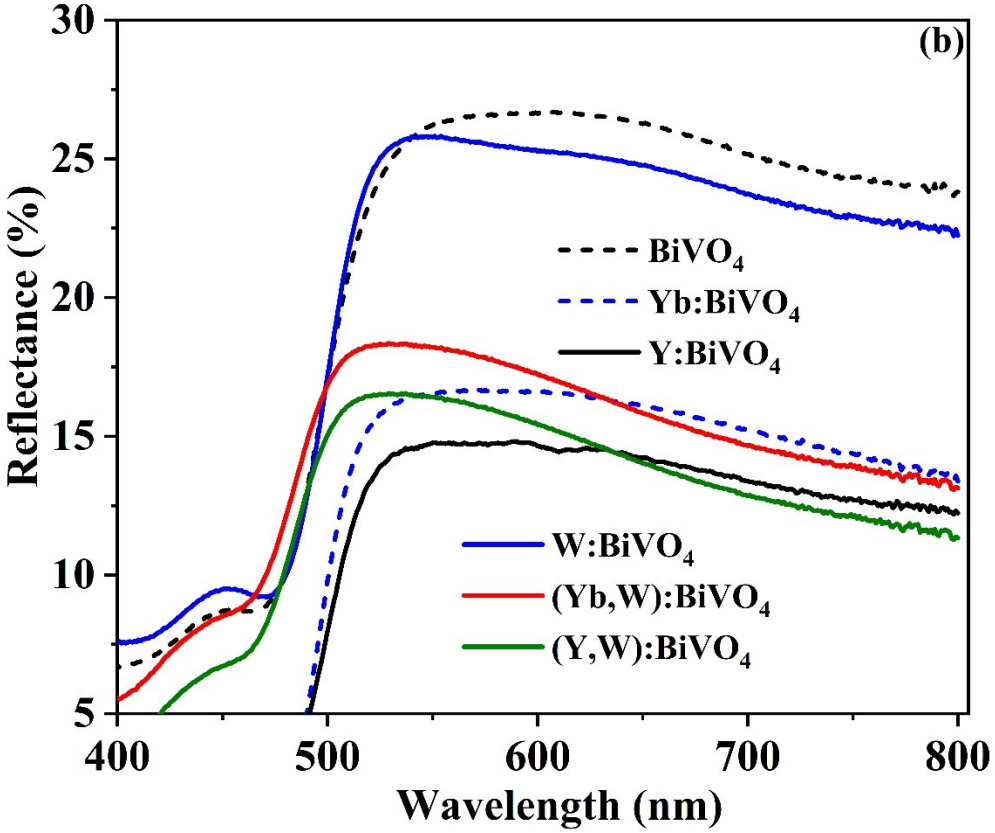
(b)
Reflectance (%)
Wavelength (nm)
30
25
20
15
10
5
400
500
600
700
800
BiVO4
Yb:BiVO4
Y:BiVO4
W:BiVO4
(Yb,W):BiVO4
(Y,W):BiVO4

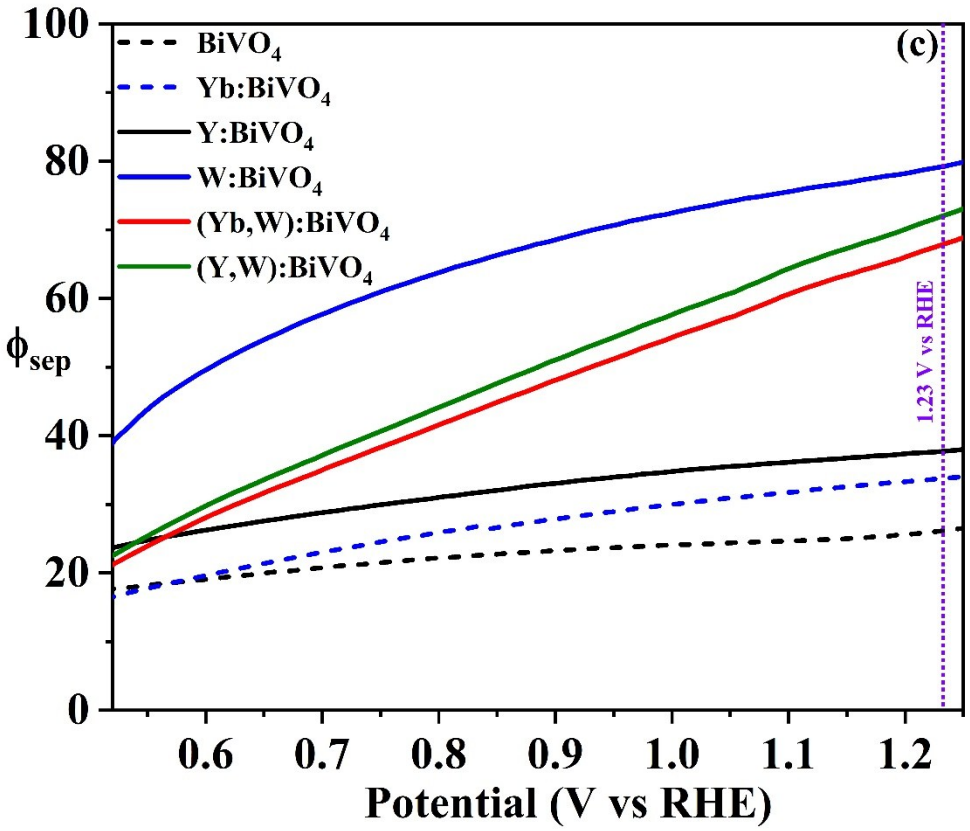
100
80
60
40
20
0
$\phi_{sep}$
0.6
0.7
0.8
0.9
1.0
1.1
1.2
Potential (V vs RHE)
(c)
BiVO4
Yb:BiVO4
Y:BiVO4
W:BiVO4
(Yb,W):BiVO4
(Y,W):BiVO4
1.23 V vs RHE

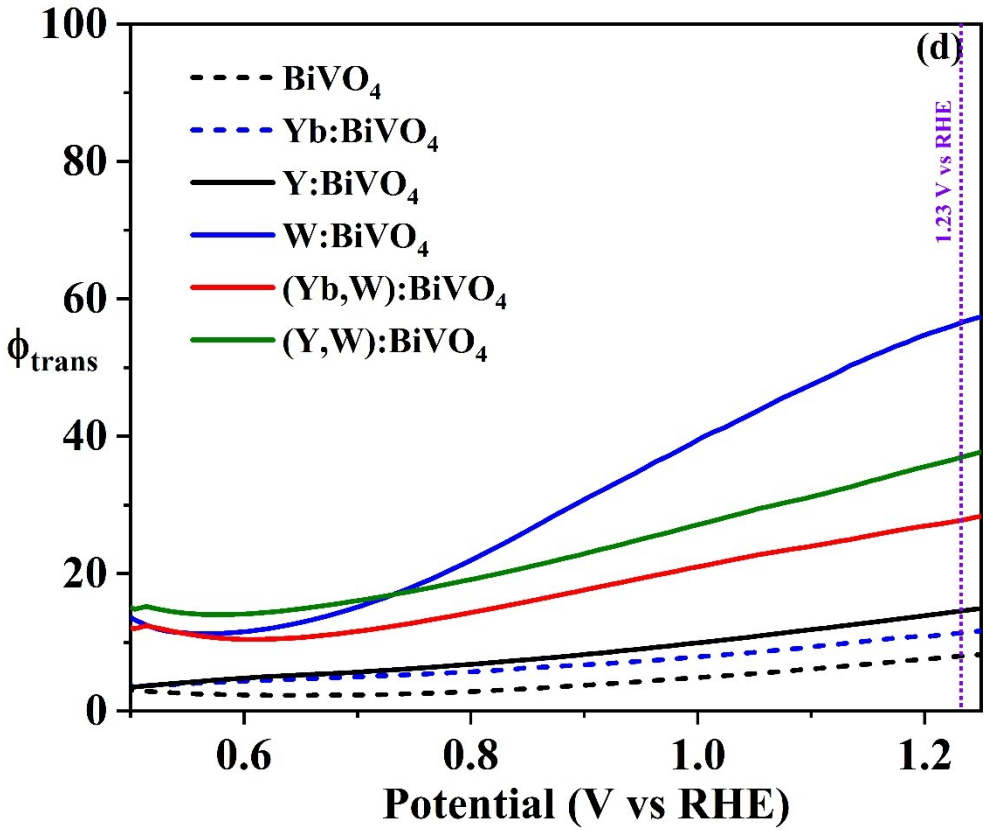
(d)
BiVO4
Yb:BiVO4
Y:BiVO4
W:BiVO4
(Yb,W):BiVO4
(Y,W):BiVO4
1.23 V vs RHE
ϕtrans
100
80
60
40
20
0
0.6
0.8
1.0
1.2
Potential (V vs RHE)

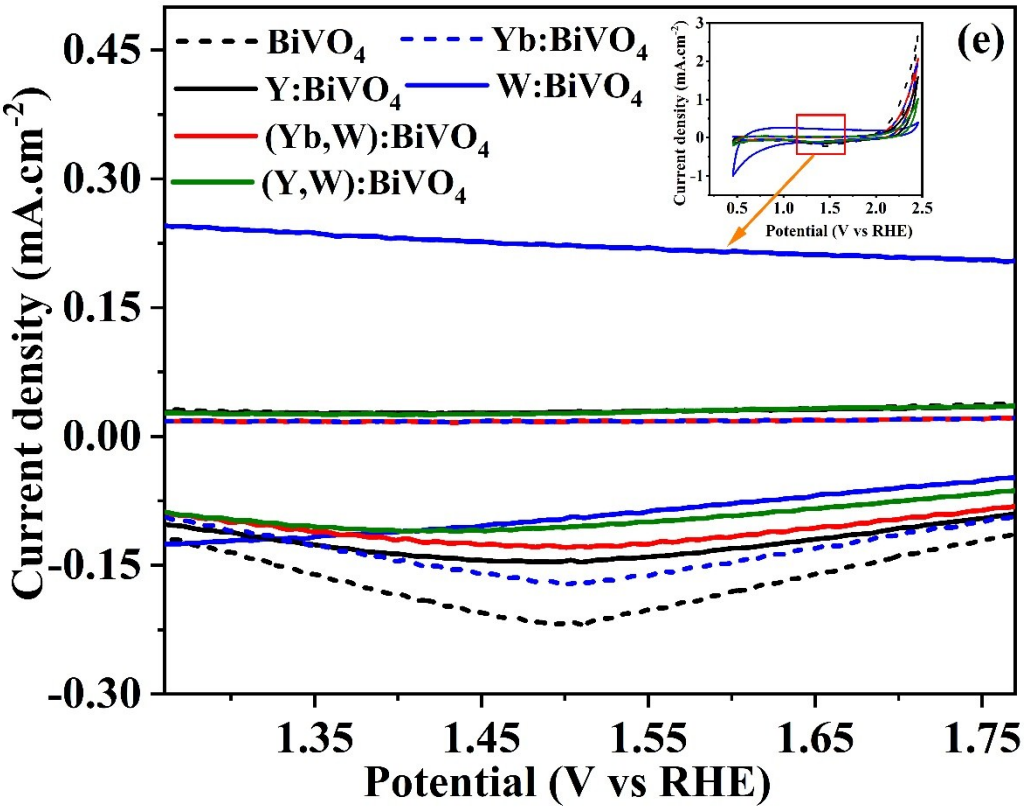


*Figure S3 (a) Calculated LHE plot, (b) reflection plot, (c) $\phi_{sep}$ plot, (d) $\phi_{trans}$ plot of pristine $BiVO_4$, $Yb:BiVO_4$, $Y:BiVO_4$, $W:BiVO_4$, $(Yb,W):BiVO_4$ and $(Y,W):BiVO_4$ photoanodes. (e) Cyclic voltammetry in dark at 20 mV/sec in 0.1 M $K_2HPO_4$.*

In order to understand the recombination center or reaction sites at the photoanode surface and electrolyte interface, CV measurement performed in $K_2HPO_4$ electrolyte from potential 0.45 to 2.5 V vs RHE in the dark (Figure S3e). The observed cathodic peak at ~1.45 V vs RHE describes the surface reaction given in eq 14[7].

$$VO_2{}^{+}\ (surface) + 2H^{+}\ (aq) + e_{inject}^{-} \rightarrow VO^{2+}\ (surface) + H_2 \qquad (14)$$

Surface reaction $VO_2^+/VO^{2+}$ is irreversible direct that charge transfer from trap sites (termed as surface state) and detrapping process is slow which lead to accumulation of charges in the trap sites and then increases recombination (eq 15)[5].

$$VO_2{}^+\ (surface) + 2H^+\ (aq) \quad \xleftrightarrow{(e^-_{photo} + h_{trap})_{recombination}} \quad VO^{2+}\ (surface) \qquad (15)$$

Since the peak potential is greater than the water oxidation potential (1.23 V vs RHE), the potential range for this state extend over the water oxidation in dark. W:$BiVO_4$ photoanodes shows smaller peak intensity compared to other photoanodes which depicts the low number of trap sites formation which lead to higher PEC performance. The peak intensity (estimated by peak ~1.45 V vs RHE fitting using Matlab software) decreasing sequence is as follows: W:$BiVO_4$ > (Y,W):$BiVO_4$ > (Yb,W):$BiVO_4$ > Y:$BiVO_4$ > Yb:$BiVO_4$ > $BiVO_4$.

The formation of heterojunction and surface OER catalyst over photoanodes revealed that the WO3/(Y,W):$BiVO_4$/Fe:NiO/Co-Pi photoanode shows the best performance rather than WO3/W:$BiVO_4$/Fe:NiO/Co-Pi. The observed phenomena is explained by the formation of recombination centers on the electrode surface (surface states) with Y/Yb doping along with W[7]. The SS has been reported to influence charge transfer at the semiconductor electrode/electrolyte interface because they can work as reaction sites and/or recombination centers on the electrode surface[8]. Doping of Y and Yb enhanced light absorption efficiency (Figure 3b) better than W doped $BiVO_4$ sample. However, there are formation of recombination centers on the $BiVO_4$ photoanode surface (surface states) with Y& Yb doping and it remain even along with W co-doping. As given in above supporting Figure S3e, the SS has been reported to influence charge transfer at the semiconductor electrode/electrolyte interface because they can work as reaction sites and/or recombination centers on the photoanode surface. The irreversible peak ($VO_2^+/VO^{2+}$ at ~ 1.45 V

vs RHE, Figure S3e) intensity values follow the order: (Yb,W):$BiVO_4$ > (Y,W):$BiVO_4$ > W:$BiVO_4$, indicating formation of large number of recombination sites for the (Yb,W):$BiVO_4$ and (Y,W):$BiVO_4$ photoanodes. This is a direct evidence for the PCD with the following order: (Yb,W):$BiVO_4$ < (Y,W):$BiVO_4$ < W:$BiVO_4$. However, after forming heterojunction ($WO_3$) and surface catalyst Fe:NiO/Co-Pi, the additional enhancement in the PCD performance of $WO_3$/(Y,W):$BiVO_4$/Fe:NiO/Co-Pi photoanode is due to effectively utilizing individual properties of Y and W in co-doped sample. The extended absorption behavior of Y (increased $\phi_{abs}$) facilitates generation of increased charge pairs, $WO_3$ film help in transfer of highly mobile electrons from bulk to FTO interface and OER catalyst layer help in increasing charge transfer at the surface electrolyte interface[5]. On the other hand, PEC performance of $WO_3$/W:$BiVO_4$ photoanode did not increase very significantly because W helps in the charge separation and generation of free charge carriers in the bulk. But there are no additional charge carriers generated as it was observed in Y or Yb doping due to extended absorption.

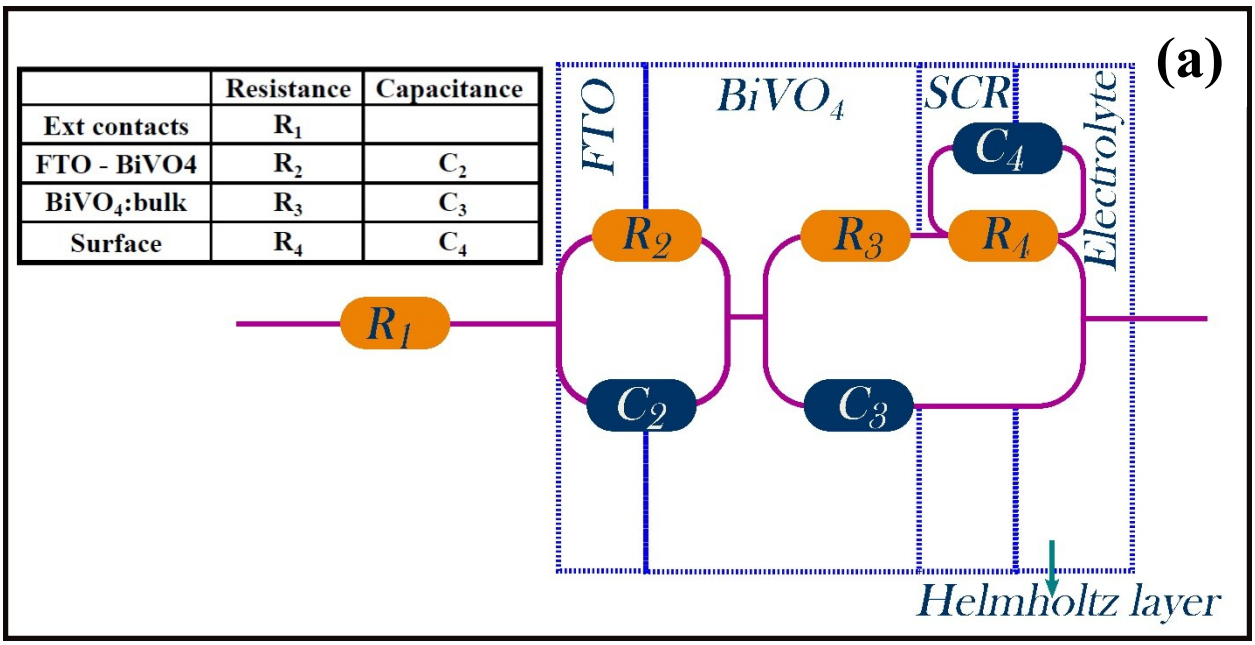
(a)
Resistance
Capacitance
Ext contacts
R1
FTO - BiVO4
R2
C2
BiVO4:bulk
R3
C3
Surface
R4
C4
FTO
BiVO4
SCR
Electrolyte
R1
R2
R3
R4
C4
C2
C3
Helmholtz layer

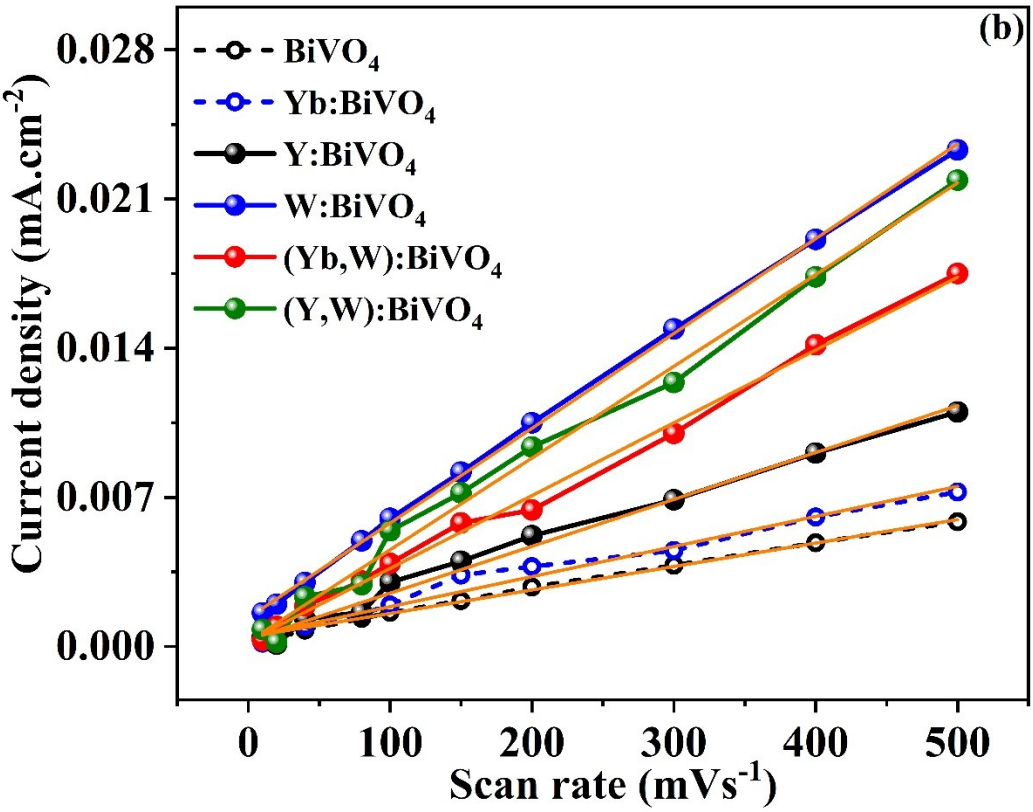
(b)
BiVO4
Yb:BiVO4
Y:BiVO4
W:BiVO4
(Yb,W):BiVO4
(Y,W):BiVO4
Current density (mA.cm-2)
0.028
0.021
0.014
0.007
0.000
0
100
200
300
400
500
Scan rate (mVs-1)

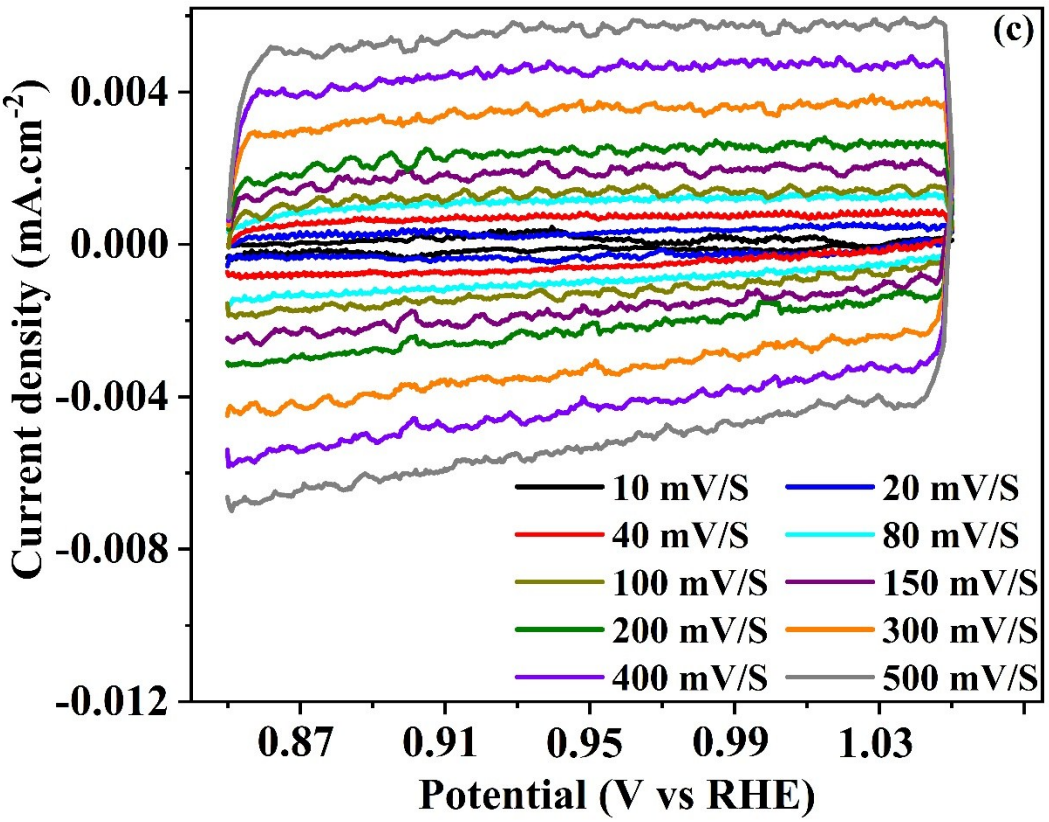
(c)
Current density (mA.cm-2)
0.004
0.000
-0.004
-0.008
-0.012
0.87
0.91
0.95
0.99
1.03
Potential (V vs RHE)
10 mV/S
20 mV/S
40 mV/S
80 mV/S
100 mV/S
150 mV/S
200 mV/S
300 mV/S
400 mV/S
500 mV/S

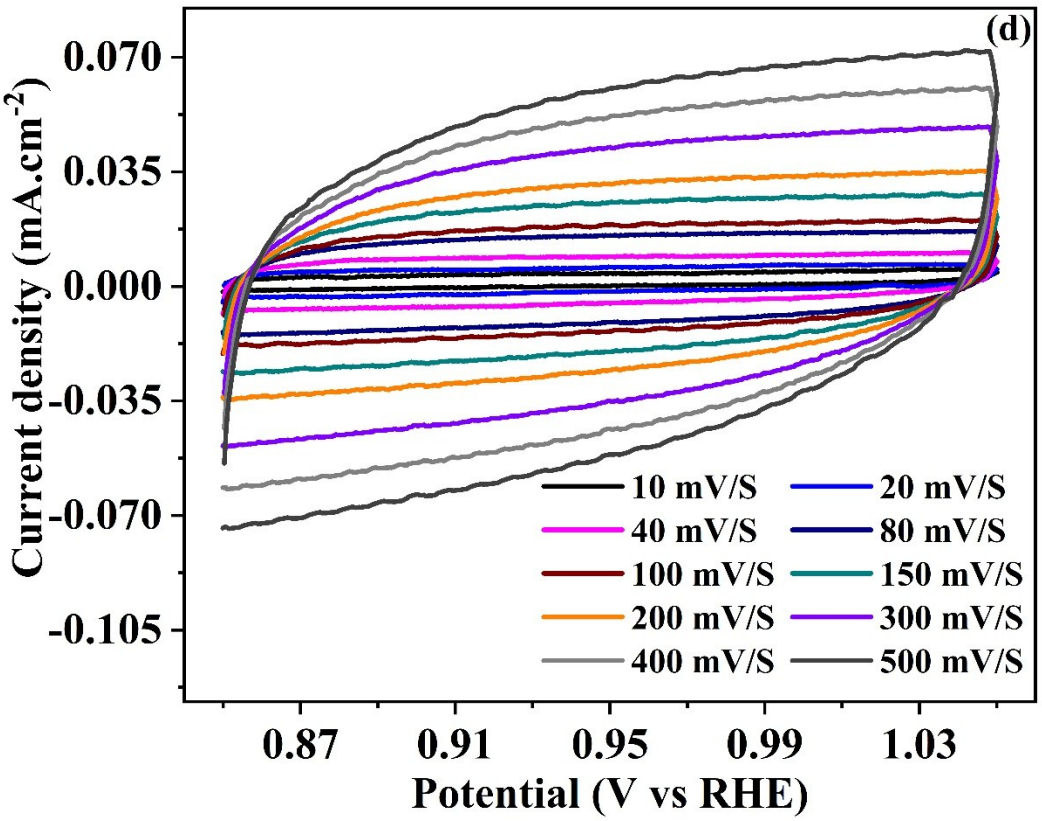
(d)
0.070
0.035
0.000
-0.035
-0.070
-0.105
Current density (mA.cm-2)
0.87
0.91
0.95
0.99
1.03
Potential (V vs RHE)
10 mV/S
20 mV/S
40 mV/S
80 mV/S
100 mV/S
150 mV/S
200 mV/S
300 mV/S
400 mV/S
500 mV/S

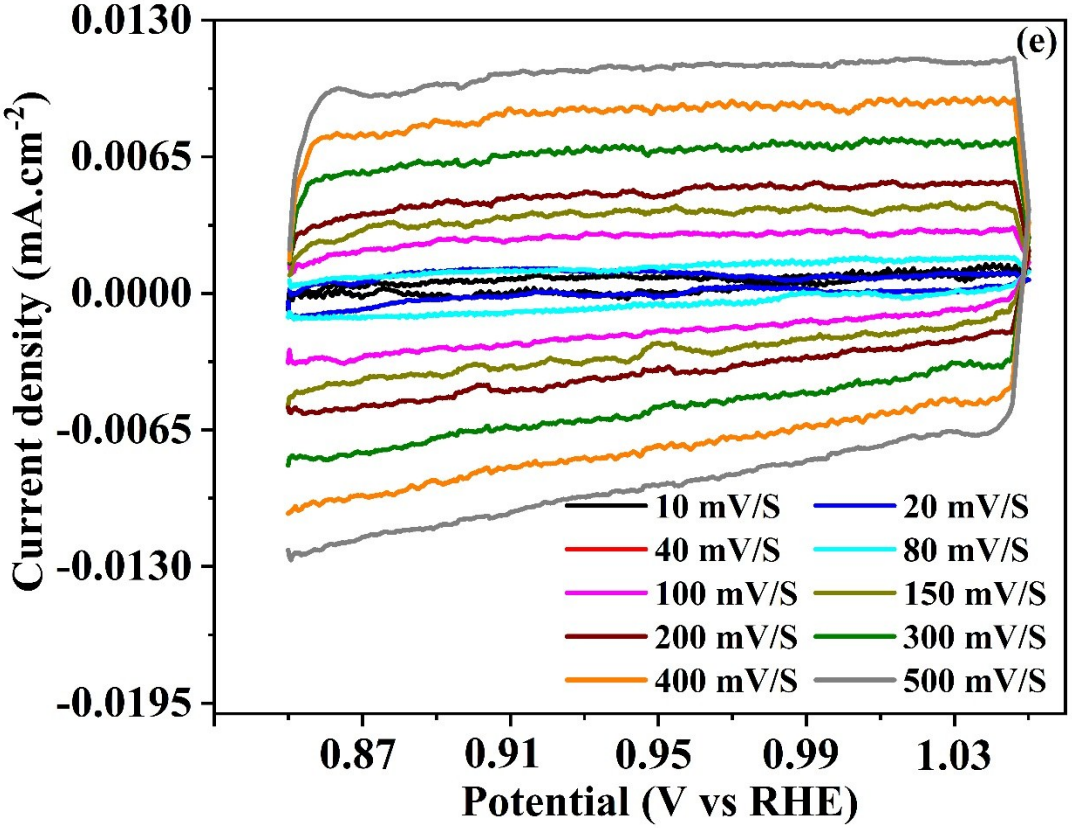
(e)
0.0130
0.0065
0.0000
-0.0065
-0.0130
-0.0195
Current density (mA.cm-2)
0.87
0.91
0.95
0.99
1.03
Potential (V vs RHE)
10 mV/S
20 mV/S
40 mV/S
80 mV/S
100 mV/S
150 mV/S
200 mV/S
300 mV/S
400 mV/S
500 mV/S

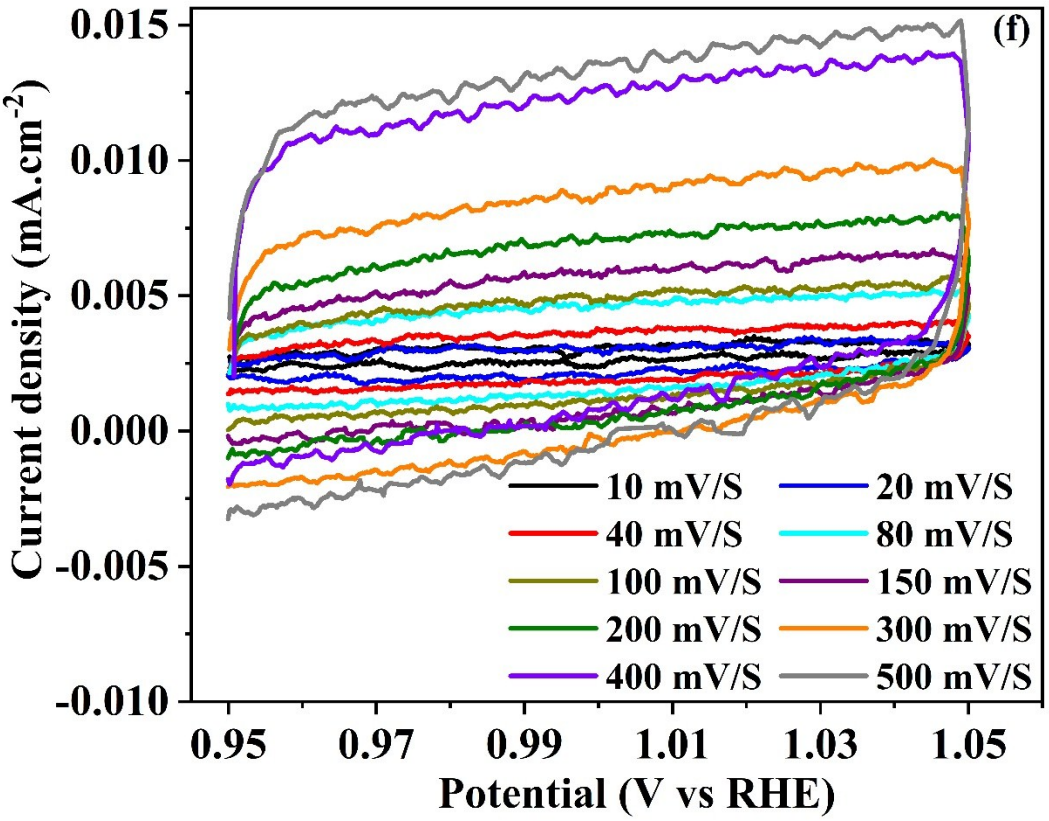
(f)
0.015
0.010
0.005
0.000
-0.005
-0.010
Current density (mA.cm-2)
0.95
0.97
0.99
1.01
1.03
1.05
Potential (V vs RHE)
10 mV/S
20 mV/S
40 mV/S
80 mV/S
100 mV/S
150 mV/S
200 mV/S
300 mV/S
400 mV/S
500 mV/S

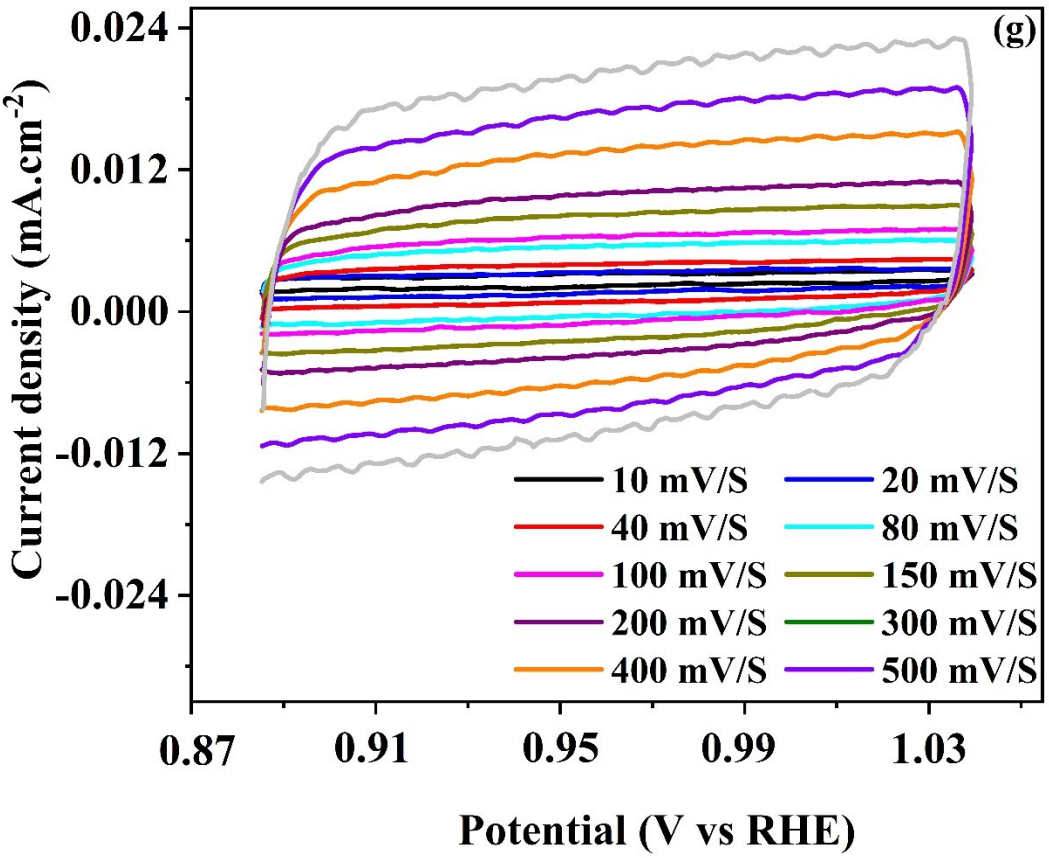
(g)
0.024
0.012
0.000
-0.012
-0.024
Current density (mA.cm-2)
0.87
0.91
0.95
0.99
1.03
Potential (V vs RHE)
10 mV/S
20 mV/S
40 mV/S
80 mV/S
100 mV/S
150 mV/S
200 mV/S
300 mV/S
400 mV/S
500 mV/S

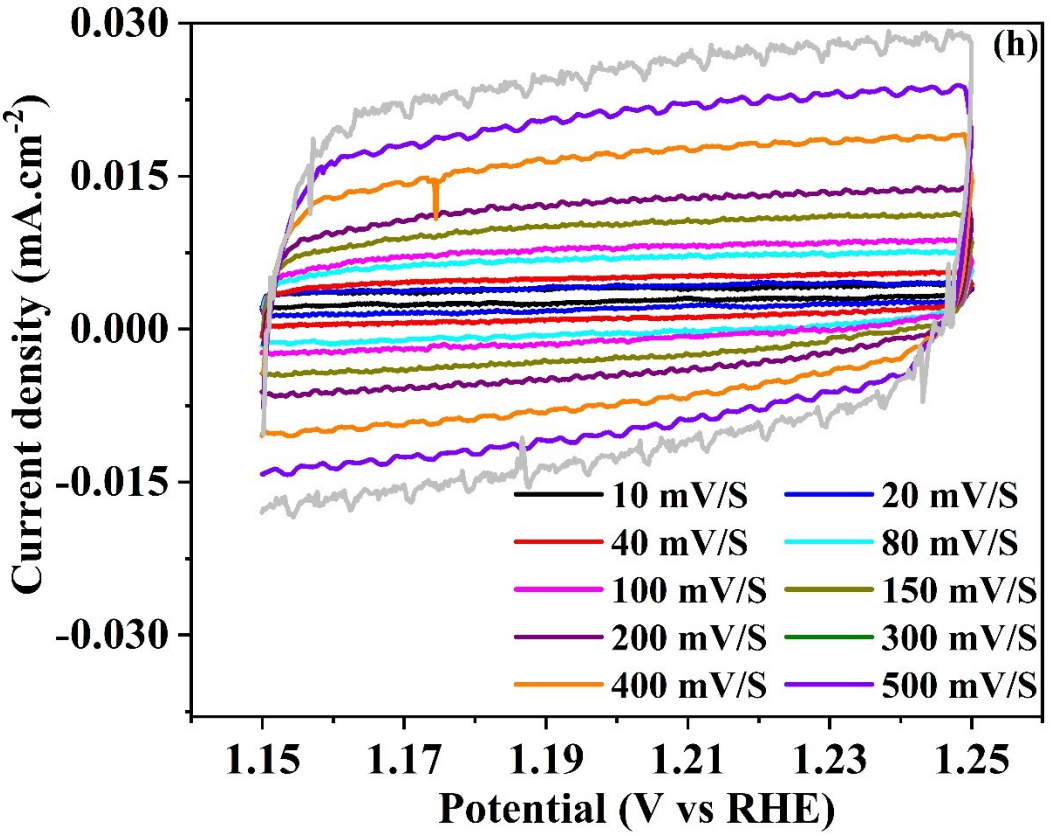


*Figure S4. (a) Equivalent Randles circuit, (b) electrochemical surface area (ECSA) plot for pristine $BiVO_4$, Yb:$BiVO_4$, Y:$BiVO_4$, W:$BiVO_4$, (Yb,W): $BiVO_4$ and (Y,W):$BiVO_4$ photoanodes. Cyclic voltammetry curves in dark for (c) pristine $BiVO_4$, (d) Yb:$BiVO_4$, (e) Y:$BiVO_4$, (f) W:$BiVO_4$, (g) (Yb,W): $BiVO_4$ and (h) (Y,W):$BiVO_4$ photoanodes. The dark current measured at 1.03 V vs RHE.*

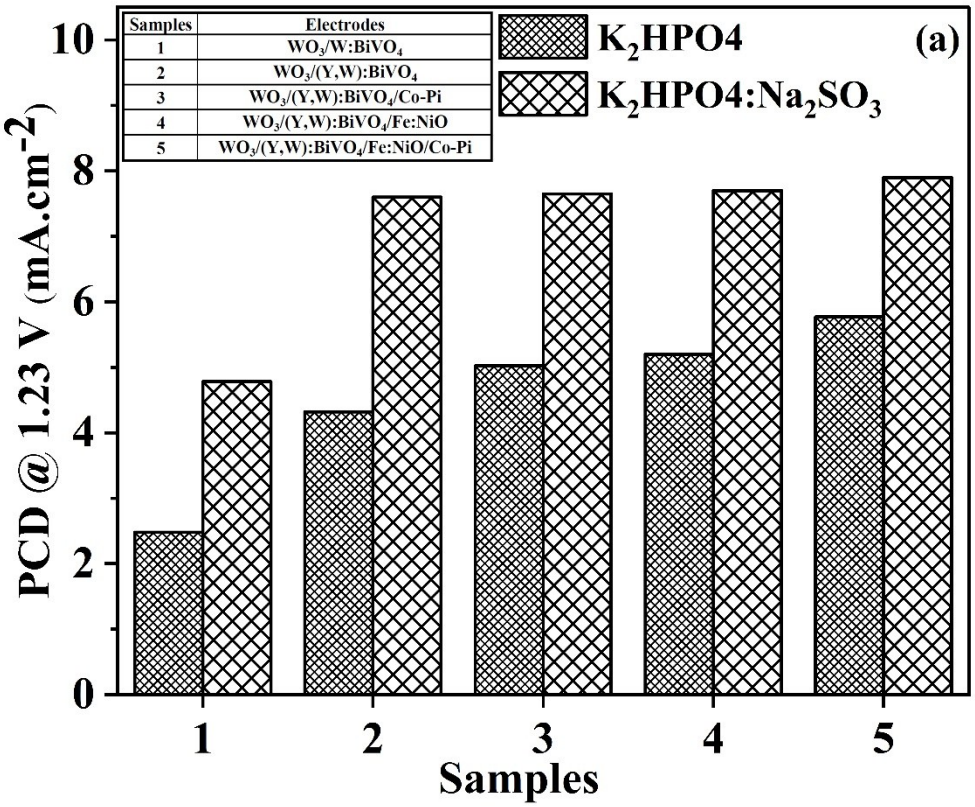
Samples
Electrodes
1
WO3/W:BiVO4
2
WO3/(Y,W):BiVO4
3
WO3/(Y,W):BiVO4/Co-Pi
4
WO3/(Y,W):BiVO4/Fe:NiO
5
WO3/(Y,W):BiVO4/Fe:NiO/Co-Pi
K2HPO4
K2HPO4:Na2SO3
(a)
PCD @ 1.23 V (mA.cm-2)
0
2
4
6
8
10
1
2
3
4
5
Samples

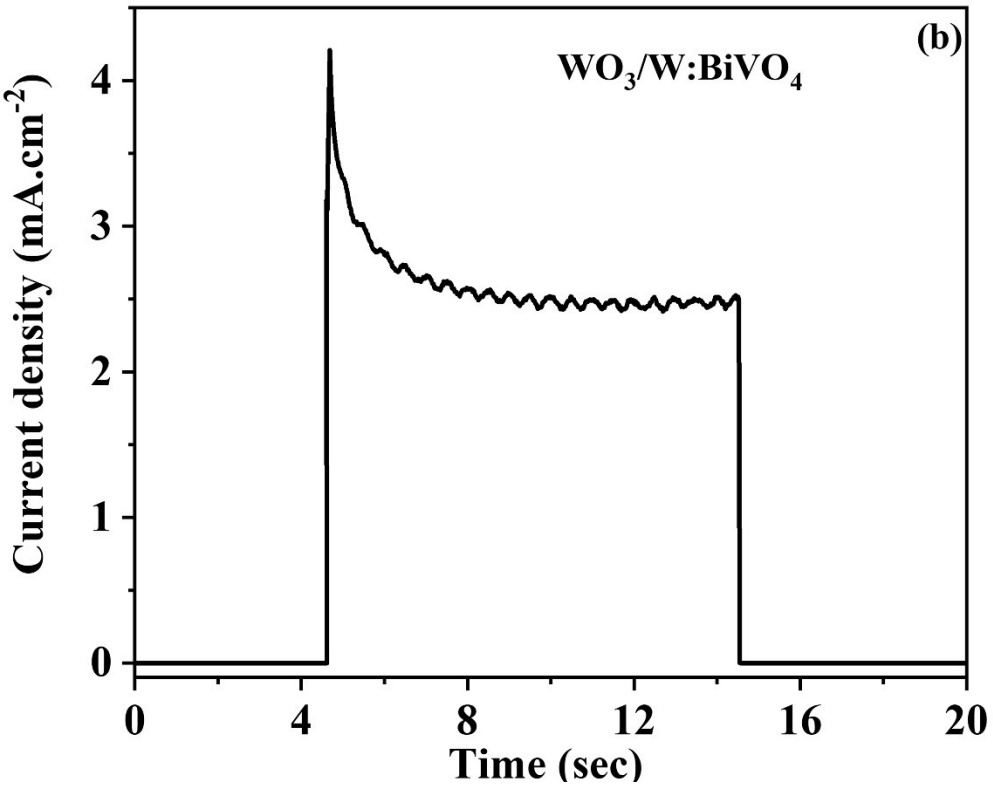
(b)
WO3/W:BiVO4
Current density (mA.cm-2)
0
1
2
3
4
0
4
8
12
16
20
Time (sec)

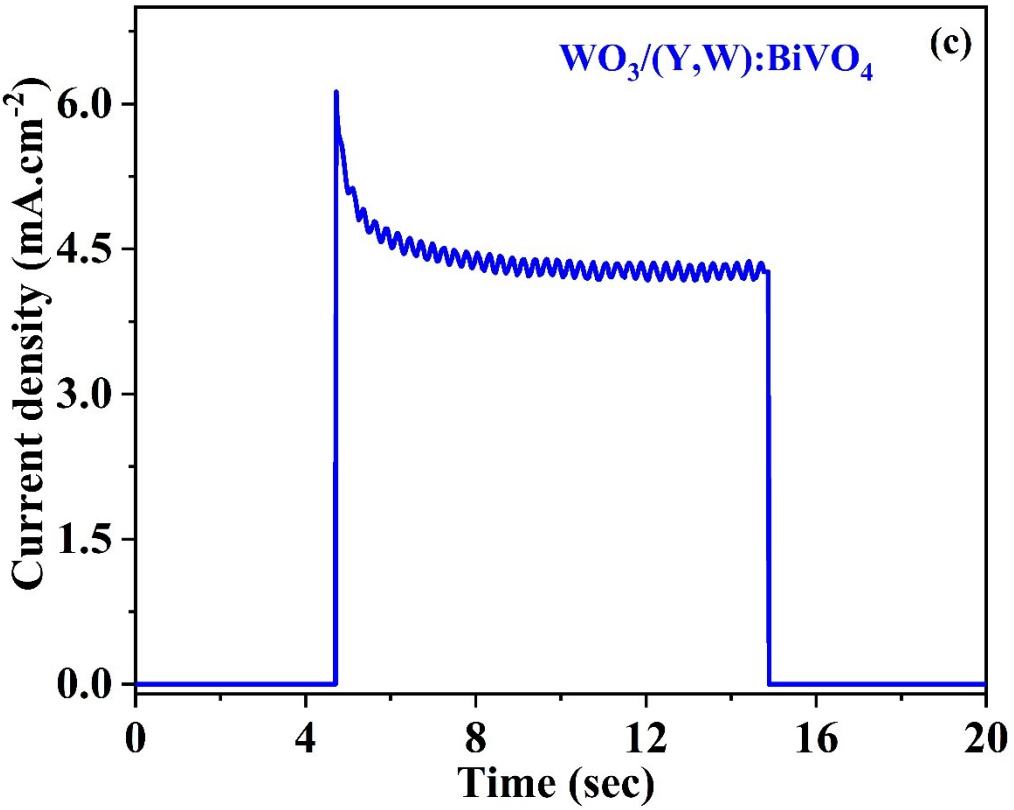
WO3/(Y,W):BiVO4
(c)
Current density (mA.cm-2)
6.0
4.5
3.0
1.5
0.0
0
4
8
12
16
20
Time (sec)

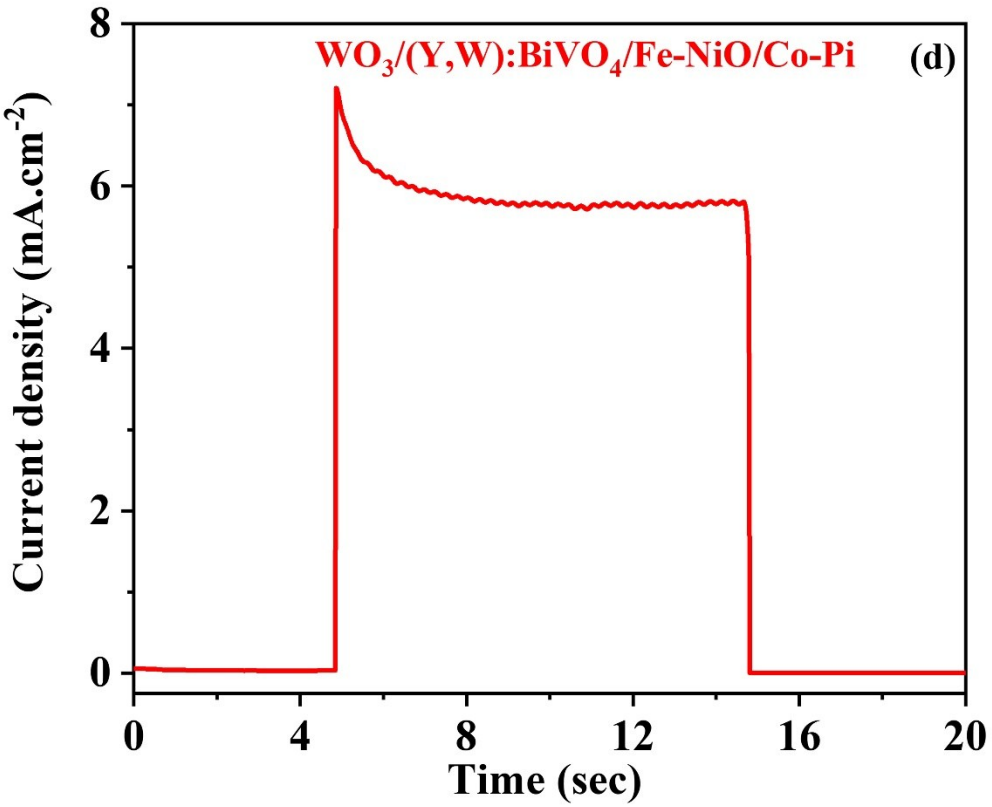
WO3/(Y,W):BiVO4/Fe-NiO/Co-Pi
(d)
Current density (mA.cm-2)
Time (sec)
0
2
4
6
8
0
4
8
12
16
20

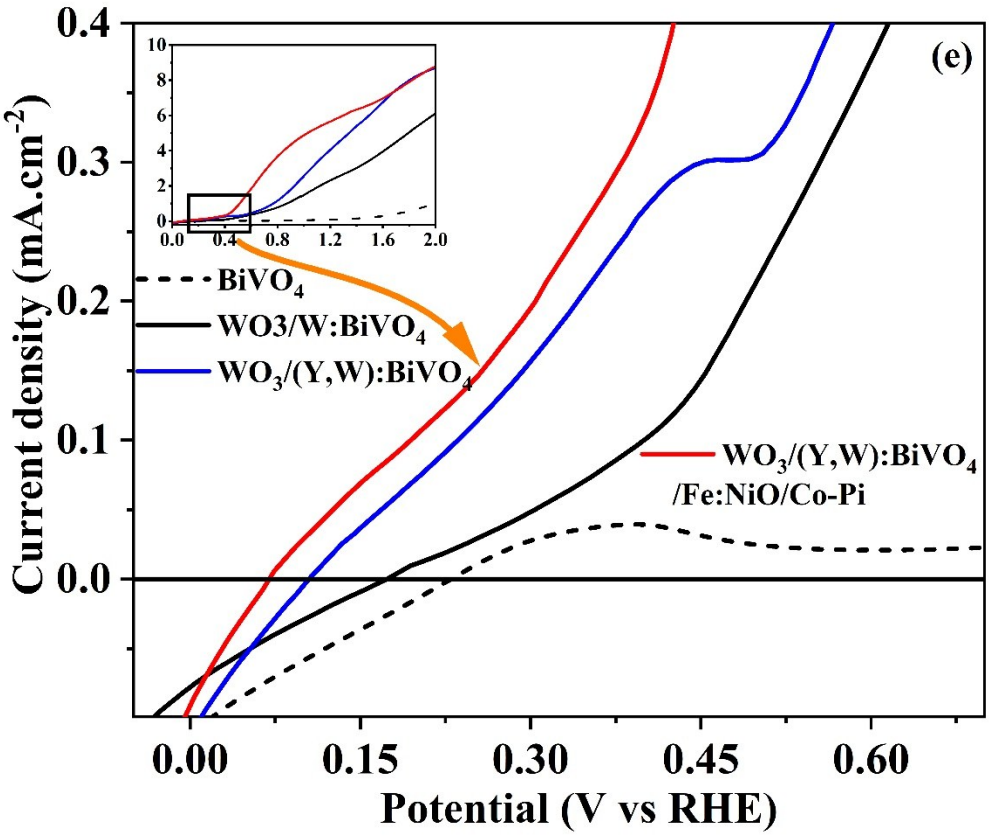
(e)
Current density (mA.cm-2)
Potential (V vs RHE)
0.4
0.3
0.2
0.1
0.0
0.00
0.15
0.30
0.45
0.60
BiVO4
WO3/W:BiVO4
WO3/(Y,W):BiVO4
WO3/(Y,W):BiVO4
/Fe:NiO/Co-Pi

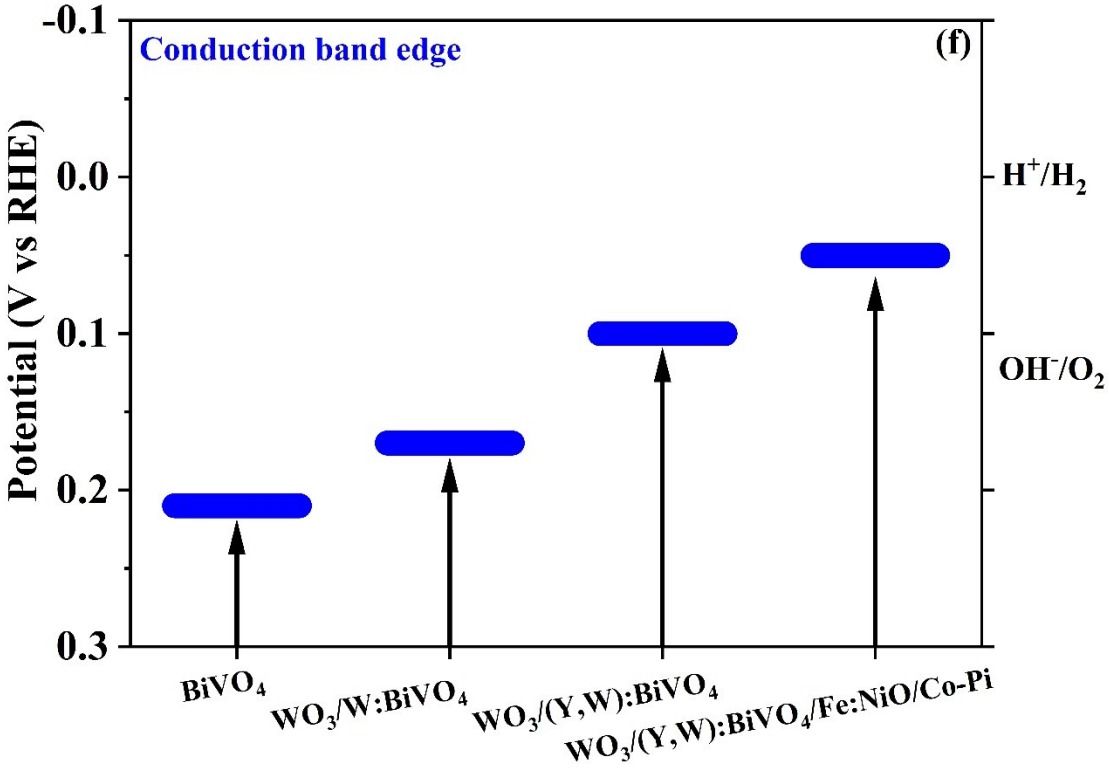
Conduction band edge
(f)
Potential (V vs RHE)
-0.1
0.0
0.1
0.2
0.3
H+/H2
OH-/O2
BiVO4
WO3/W:BiVO4
WO3/(Y,W):BiVO4
WO3/(Y,W):BiVO4/Fe:NiO/Co-Pi

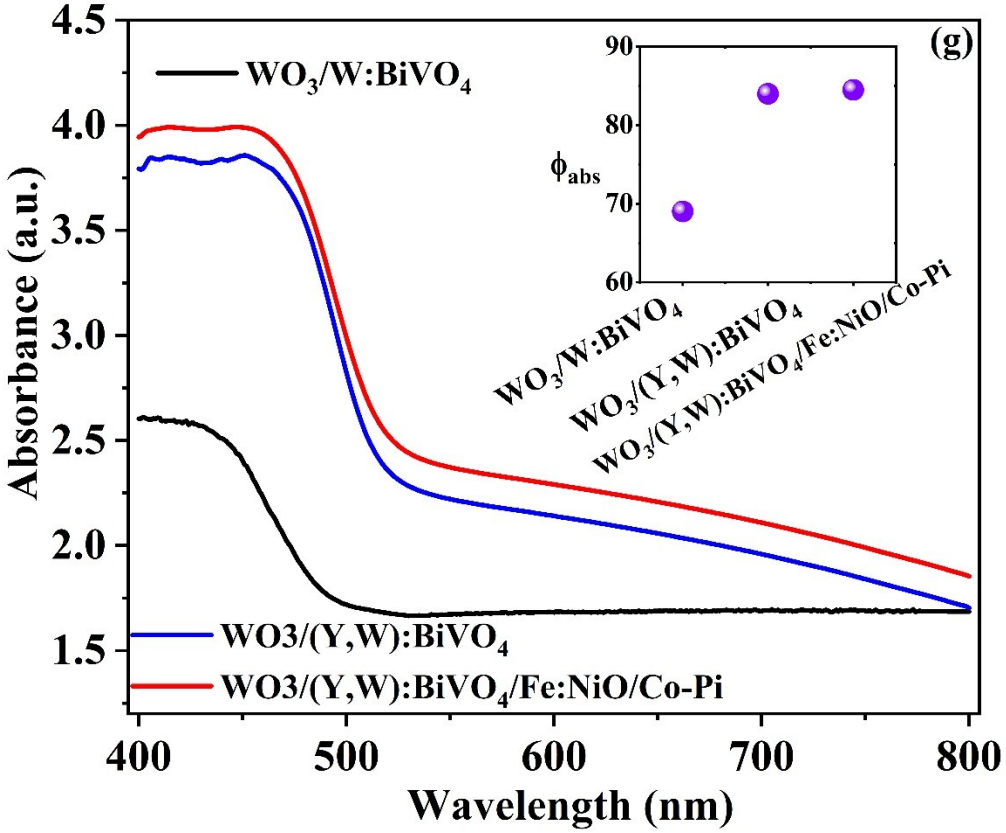
(g)
WO3/W:BiVO4
WO3/(Y,W):BiVO4
WO3/(Y,W):BiVO4/Fe:NiO/Co-Pi
Absorbance (a.u.)
Wavelength (nm)
ϕabs
WO3/W:BiVO4
WO3/(Y,W):BiVO4
WO3/(Y,W):BiVO4/Fe:NiO/Co-Pi

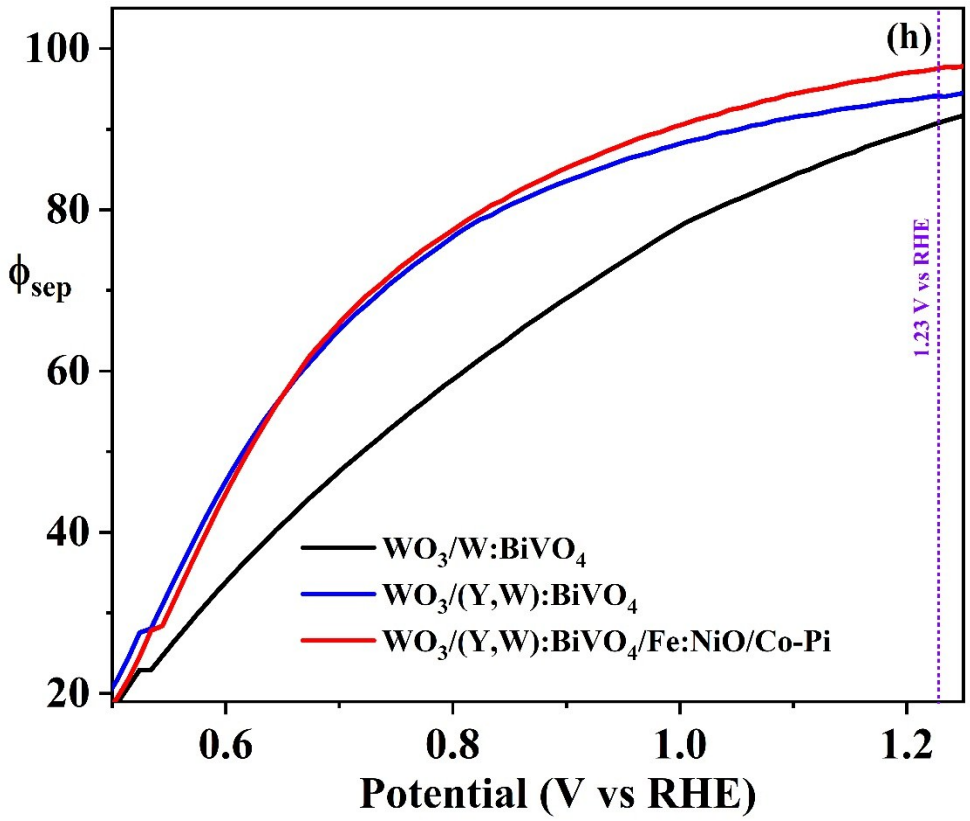
(h)
100
80
60
40
20
$\phi_{sep}$
0.6
0.8
1.0
1.2
Potential (V vs RHE)
1.23 V vs RHE
$WO_3$/W:$BiVO_4$
$WO_3$/(Y,W):$BiVO_4$
$WO_3$/(Y,W):$BiVO_4$/Fe:NiO/Co-Pi

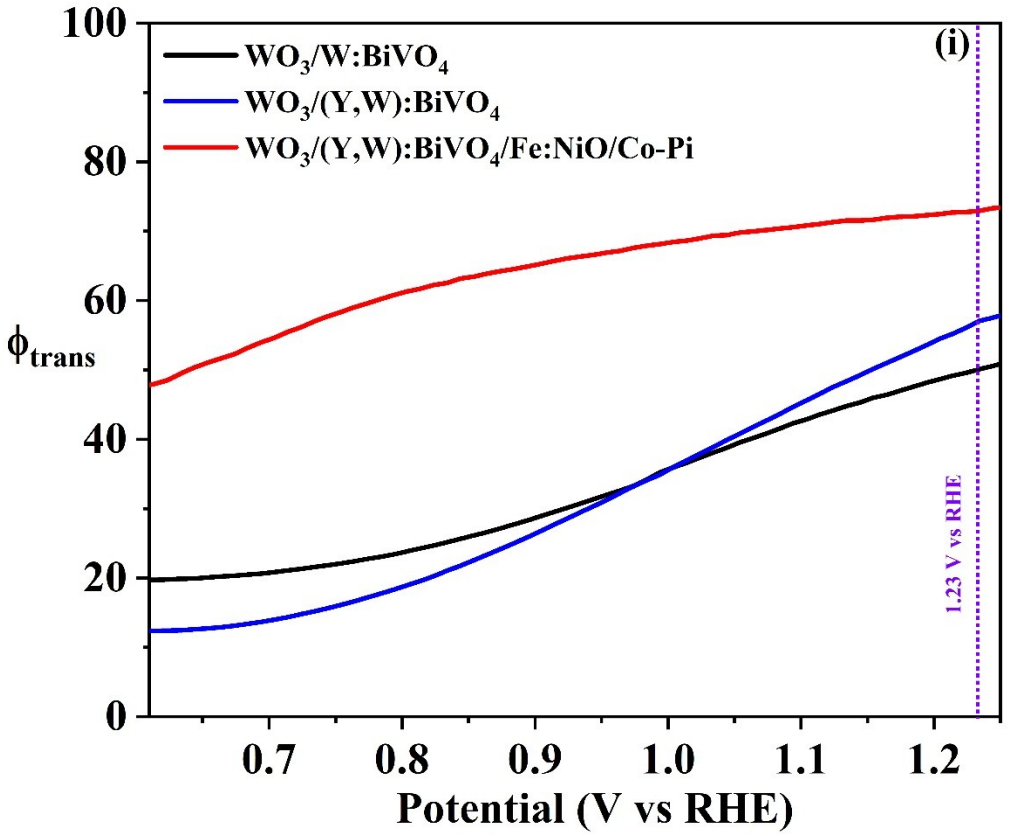


*Figure S5. (a) PCD values after catalyst Fe:NiO and Co-Pi at 1.23 V vs RHE. (b-d) Transient current plots measured for 10 sec at 1.23 V vs RHE in 0.1 M $K_2HPO_4$ electrolyte at 1sun illumination, (e) current onset plot, (f) shift in conduction band edge for $BiVO_4$, $WO_3$/W:$BiVO_4$, $WO_3$/(Y,W):$BiVO_4$ and $WO_3$/(Y,W):$BiVO_4$/Fe:NiO/Co-Pi photoanode, (g) UV-vis absorption spectra, absorption efficiency (inset), (h) $\phi_{sep}$ plot, (i) $\phi_{trans}$ plot for $WO_3$/W:$BiVO_4$, $WO_3$/(Y,W):$BiVO_4$ and $WO_3$/(Y,W):$BiVO_4$/Fe:NiO/Co-Pi photoanodes.*

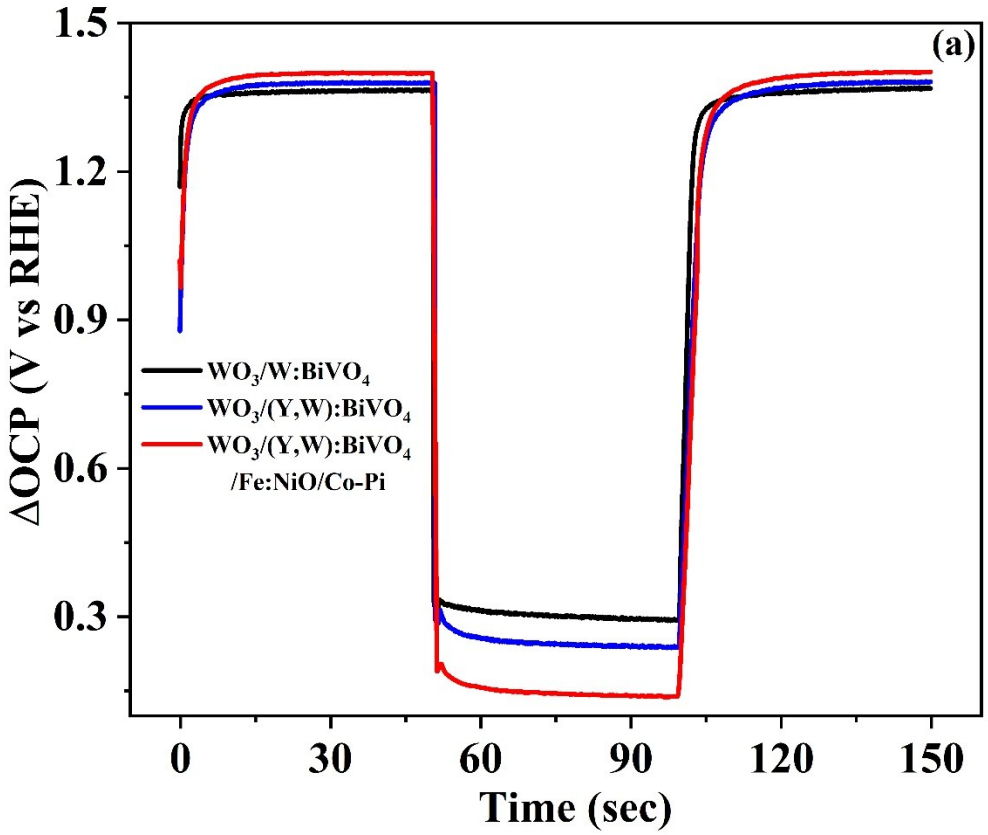
(a)
ΔOCP (V vs RHE)
1.5
1.2
0.9
0.6
0.3
0
30
60
90
120
150
Time (sec)
WO3/W:BiVO4
WO3/(Y,W):BiVO4
WO3/(Y,W):BiVO4
/Fe:NiO/Co-Pi

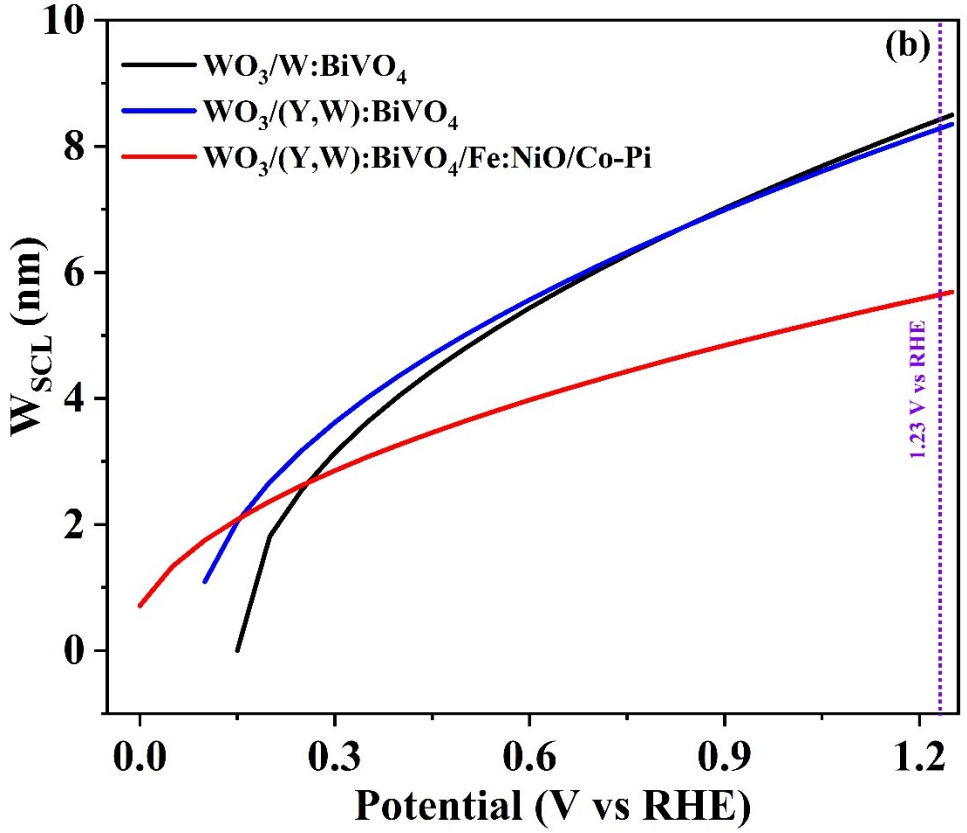


*Figure S6 (a) Open circuit potential (ΔOCP), (b) space charge width (SCL) plot for $WO_3$/W:$BiVO_4$, $WO_3$/(Y,W):$BiVO_4$ and $WO_3$/(Y,W):$BiVO_4$/Fe:NiO/Co-Pi photoanodes.*

*Table S1. Cell parameters evaluated from Rietveld refinement for pristine $BiVO_4$, Yb:$BiVO_4$, Y:$BiVO_4$, W:$BiVO_4$, (Yb,W): $BiVO_4$ and (Y,W):$BiVO_4$ samples.*

| Photoanode | Lattice parameter, a (Å) | Lattice parameter, b (Å) | Lattice parameter, c (Å) | Angle (Degree) | Volume, (Å $^3$) |
|---|---|---|---|---|---|
| $BiVO_4$ | 5.1758 | 5.1079 | 11.6707 | 89.9270 | 308.5515 |
| Yb:$BiVO_4$ | 5.1759 | 5.1002 | 11.6811 | 89.9985 | 308.3630 |
| Y:$BiVO_4$ | 5.1808 | 5.1034 | 11.6579 | 89.9905 | 308.2370 |
| W:$BiVO_4$ | 5.1759 | 5.1042 | 11.6743 | 89.9975 | 308.42133 |
| (Yb,W):$BiVO_4$ | 5.1768 | 5.09729 | 11.6841 | 89.9990 | 308.3204 |
| (Y,W):$BiVO_4$ | 5.1808 | 5.1034 | 11.6571 | 89.9989 | 308.2101 |

*Table S2. Calculated parameters pristine $BiVO_4$, Yb:$BiVO_4$, Y:$BiVO_4$, W:$BiVO_4$, (Yb,W): $BiVO_4$ and (Y,W):$BiVO_4$ photoanodes.*

| Photoanodes | $J_{theoretical}$ (mA.cm-2) | $\phi_{abs}$ (%) | $\phi_{sep}$ (%) | $\phi_{trans}$ (%) | $\phi_{abs} \times \phi_{sep} \times \phi_{trans}$ (%) | Band gap (eV) |
|---|---|---|---|---|---|---|
| $BiVO_4$ | 7.5 | 62 ± 3 | 26 ± 1.4 | 8 ± 0.4 | 1.29 ± 0.07 | 2.51 |
| Yb:$BiVO_4$ | 9.6 | 68 ± 3.2 | 34 ± 1.8 | 12 ± 0.5 | 2.77 ± 0.14 | 2.37 |
| Y:$BiVO_4$ | 9.6 | 73 ± 4 | 38 ± 2 | 14 ± 0.8 | 3.88 ± 0.2 | 2.29 |
| W:$BiVO_4$ | 7.5 | 63 ± 3.1 | 79.5 ± 4 | 55 ± 2.8 | 27.55 ± 1.38 | 2.51 |
| (Yb,W):$BiVO_4$ | 9.6 | 71 ± 3.5 | 67.5 ± 3.4 | 28 ± 1.5 | 13.42 ± 0.7 | 2.37 |
| (Y,W):$BiVO_4$ | 9.6 | 77 ± 3.9 | 73 ± 4 | 36 ± 1.8 | 20.24 ± 1 | 2.29 |

| $R_b$ (kΩ) | $R_s$ (kW) | $C_b$ (μF) | $C_s$ (μF) | $A_{ECSA}$ ($cm^2$) | $N_D$ ($cm^{-3}$) | PCD (mA.$cm^{-2}$) |
|---|---|---|---|---|---|---|
| 2.1 ± 0.1 | 4.33 ± 0.22 | 409 ± 20.4 | 36.5 ± 1.9 | 0.44 ± 0.024 | 2.8916E+19 | 0.095 ± 0.005 |
| 1.82 ± 0.094 | 3.81 ± 0.19 | 242 ± 12.5 | 83.2 ± 4.2 | 0.56 ± 0.03 | 3.0116E+19 | 0.26 ± 0.013 |
| 1.64 ± 0.083 | 3.62 ± 0.18 | 173 ± 8.7 | 190 ± 9.5 | 0.68 ± 0.035 | 3.7816E+19 | 0.37 ± 0.17 |
| 0.48 ± 0.025 | 0.85 ± 0.043 | 5.4 ± 0.45 | 410 ± 20.5 | 1.16 ± 0.06 | 1.07236E+20 | 2.2 ± 0.13 |
| 0.51 ± 0.056 | 1.19 ± 0.06 | 8.3 ± 0.52 | 334 ± 17 | 0.92 ± 0.1 | 9.62267E+19 | 1.29 ± 0.06 |
| 0.49 ± 0.024 | 0.96 ± 0.05 | 6.27 ± 0.48 | 387 ± 20 | 1.05 ± 0.055 | 1.04236E+20 | 1.94 ± 0.1 |

*Table S3. Calculated parameters $WO_3$/W:$BiVO_4$, $WO_3$/(Y,W):$BiVO_4$ and $WO_3$(Y,W):$BiVO_4$/Fe:NiO/Co-Pi photoanodes.*

| Photoanodes | $J_{theoretical}$ (mA.cm-2) | $\phi_{abs}$ (%) | $\phi_{sep}$ (%) | $\phi_{trans}$ (%) | $\phi_{abs} \times \phi_{sep} \times \phi_{trans}$ (%) | Total charge recobine (%) | $N_D$ ($cm^{-3}$) |
|---|---|---|---|---|---|---|---|
| $BiVO_4$ | | | | | | 90 ± 5 | 2.8916E+19 |
| $WO_3$/W:$BiVO_4$ | 7.5 | 71 ± 3.6 | 92 ± 4.8 | 50.5 ± 2.5 | 33 ± 2.5 | 42 ± 2 | 1.14522E+20 |
| $WO_3$/(Y,W):$BiVO_4$ | 9.6 | 84 ± 4.5 | 94 ± 4.7 | 57 ± 3 | 45 ± 2.9 | 31 ± 2 | 1.26141E+20 |
| $WO_3$/(Y,W):$BiVO_4$/Fe:NiO/Co-Pi | 9.6 | 84 ± 4.5 | 98 ± 5 | 73 ± 4 | 60 ± 3.7 | 19 ± 1.2 | 2.95041E+20 |

| $V_{onset}$ (V vs RHE) | $V_{FB}$ (V vs RHE) | ΔOCP (V vs RHE) | $W_{SCL}$ (nm) | Band Bending (mV vs RHE) | $A_{ECSA}$ ($cm^2$) | IPCE (%) |
|---|---|---|---|---|---|---|
| 0.23 | 0.21 | | 16.24 | 0 ± 0 | | 3.3 ± 0.17 |
| 0.18 | 0.15 | 0.3 | 8.43 | 35.34 ± 1.8 | 1.2 ± 0.025 | 45 ± 2.15 |
| 0.11 | 0.08 | 0.24 | 8.29 | 37.83 ± 1.9 | 1.35 ± 0.08 | 73 ± 3 |
| 0.07 | 0.03 | 0.15 | 5.67 | 60 ± 0.3 | 1.46 ± 0.1 | 97 ± 4.5 |

| APCE (%) | $J_{Integrated}$ (mA.cm-2) | PCD ($mA.cm^{-2}$) | PCD with hole scavangers ($mA.cm^{-2}$) |
|---|---|---|---|
| 4 ± 0.18 | 0.15 ± 0.0075 | | |
| 51 ± 2.5 | 2.6 ± 0.15 | 2.48 ± 0.12 | 4.78 ± 0.28 |
| 82 ± 2.6 | 4.38 ± 0.22 | 4.32± 0.22 | 7.6 ± 0.4 |
| ~ 98 | 5.81 ± 0.3 | 5.77 ± 0.3 | 7.8 ± 0.5 |

**Supplementary reference:**


1 J. Jia, L. C. Seitz, J. D. Benck, Y. Huo, Y. Chen, J. W. D. Ng, T. Bilir, J. S. Harris and T. F. Jaramillo, *Nat. Commun.*, 2016, **7**, 1–6.

2 U. Prasad, J. Prakash, B. Azeredo and A. Kannan, *Electrochim. Acta*, 2019, **299**, 262–272.

3 Y. Ma, S. R. Pendlebury, A. Reynal, F. Le Formal and J. R. Durrant, *Chem. Sci.*, 2014, **5**, 2964–2973.

4 W. He, R. Wang, C. Zhou, J. Yang, F. Li and X. Xiang, *Ind. Eng. Chem. Res.*, 2015, **54**, 10723–10730.

5 U. Prasad, J. Prakash, S. K. Gupta, J. Zuniga, Y. Mao, B. Azeredo and A. N. M. Kannan, *ACS Appl. Mater. Interfaces*, 2019, **11**, 19029–19039.

6 F. F. Abdi, L. Han, A. H. M. Smets, M. Zeman, B. Dam and R. Van De Krol, *Nat. Commun.*, 2013, **4**, 1–7.

7 Q. Shi, S. Murcia-López, P. Tang, C. Flox, J. R. Morante, Z. Bian, H. Wang and T. Andreu, *ACS Catal.*, 2018, **8**, 3331–3342.

8 S. Trasa, A. Petrii and K. Niki, *J. N. Agar (UK J. Koryta (Czechoslovakia Plieth (FRG*, 1992, **321**, 353–376.